International Journal of Hydrogen Energy 135 (2025) 537–552

Contents lists available at ScienceDirect

International Journal of Hydrogen Energy

journal homepage: www.elsevier.com/locate/he

Comparative performance assessment of multilayer insulation (MLI) systems for liquid hydrogen vessels in fire scenarios

Davide Camplese [a], Giordano Emrys Scarponi [a], Robert Eberwein [b], Aliasghar Hajhariri [b], Frank Otremba [b], Valerio Cozzani [a,*]

[a] LISES - Department of Civil, Chemical, Environmental and Material Engineering, Alma Mater Studiorum – University of Bologna, Via Terracini 28, 40131, Bologna, Italy

[b] BAM – Department of Tanks for the Storage of Dangerous Goods and Accident Mechanics, Unter Den Eichen 87, 12205, Berlin, Germany

ARTICLE INFO

Handling Editor: M Djukic

Keywords:
Multilayer insulation
Hydrogen
Liquid hydrogen
Fire safety
Cryogenic tanks
Key performance indicators

ABSTRACT

Multilayer Insulation (MLI) systems are a mature technology for cryogenic liquid hydrogen (LH_2) tank thermal insulation. Recent tests evidenced that MLI materials may be damaged when exposed to fire, resulting in critical safety issues in the case of accidents. Thus, an innovative approach to the performance assessment of aluminum and polyester-based MLIs for LH_2 tanks in fire scenarios was developed. A specific model integrating the high-temperature degradation of MLIs and the thermodynamic modeling of the tank lading was coupled to specific key performance indicators. Results of the analysis applied to a vehicle-scale tank equipped with 80 MLI layers indicate that MLI degradation and consequent tank failure may occur in less than 20 min for external shell temperatures above 1160 K in the presence of full engulfment, regardless of insulation used. Conversely, degradation does not occur earlier than 3600s below 603 and 928 K for polyester and aluminum-based MLI, respectively.

Nomenclature

A	preexponential factor, 1/s
A_L	liquid-wetted surface area, m^2
A_{PRV}	PRV opening section, m^2
A_{Si}	inner shell surface area, m^2
A_V	vapor-wetted surface area, m^3
C_2	empirical constant for the spacer material, -
cp	specific heat capacity at constant pressure, J/(kg·K)
D	tank diameter, m
D_x	spacer thickness, m
E_a	activation energy, J/mol
f	relative density of the spacer to the solid spacer material, -
g	gravitational acceleration, m^2/s
Gr	Grashof number, -
h	heat transfer coefficient, $W/(m^2*K)$
H	characteristic length of the vacuum enclosure, m
$\dot{H}_{PRV}$	specific enthalpy of hydrogen vapor outflowing from the PRV, J/kg
k	thermal conductivity, W/(m·K)
K_d	PRV discharge coefficient, -
L	tank length, m
m	mass, kg
$\dot{m}$	mass flow, kg/s

(*continued on next column*)

(*continued*)

M	molecular weight, kg/mol
n	reaction order, -
N	number of radiative layers, -
Nu	Nusselt number, -
P	pressure within the tank (absolute), Pa
P_g	gauge pressure within the tank, Pa
P_o	pressure at PRV outlet, Pa (101325 Pa)
$P_{PRV,\ open}$	PRV opening pressure, Pa
$P_{PRV,\ close}$	PRV closing pressure, Pa
P_r	residual gas pressure, Pa
Pr	Prandtl number, -
q	heat flux, kW/m^2
Q	thermal power, W
R	universal gas constant, J/(mol·K)
Ra	Rayleigh number, -
t	time, s
t_{od}	onset of degradation time, s
t_{td}	total degradation time, s
t_{PRV}	time of the first PRV opening, s
ttf	time to mechanical failure of the tank, s
T	temperature, K
$\overline{T}$	average temperature between two adjacent MLI reflective layers, K

(*continued on next page*)

* Corresponding author.
E-mail address: valerio.cozzani@unibo.it (V. Cozzani).

https://doi.org/10.1016/j.ijhydene.2025.04.534
Received 24 November 2024; Received in revised form 6 April 2025; Accepted 30 April 2025
Available online 9 May 2025

(*continued*)

$\hat{U}$	specific internal energy, J/kg
V_{Si}	volume of the inner tank, m^3
Y_s	solid mass at instant t normalized on the initial value, -
Greek letters	
α	coefficient of volume expansion, K^{-1}
β	heating rate, K/min
γ	heat capacity ratio, -
δ	thickness, m
ε	emissivity of the material surface, -
ζ	atomic degrees of freedom of the gas (it equals 2 for air and nitrogen), -
θ	accommodation factor, -
ν	kinematic viscosity, m^2/s
μ	dynamic viscosity, Pa·s
ρ	density, kg/m^3
σ	Stefan-Boltzmann coefficient, $W/(m^2 \cdot K^4)$
σ_v	equivalent mechanical stress, Pa
σ_y	yield strength, Pa
σ_l	longitudinal primary stress, Pa
σ_h	circumferential primary stress, Pa
σ_r	radial primary stress, Pa
ϕ	weight factor, -
ψ_f	dumping factor for standard fire curve correlation, -
Δx	vacuum gap thickness between the double walls of the tank, -
Abbreviations	
CFD	Computational fluid dynamics
LH2	Liquefied hydrogen
MLI	Multilayer insulation
PRV	Pressure relief valve
KPI	Key performance indicator
RT	Reference time
Subscripts and Superscripts	
cond	conduction
conv	convection
exp	experimental
f	fire
g	gas
i	i-th reflective layer
H_2	hydrogen fluid
L	liquid
N	outermost reflective layer
rad	radiation
rl	reflective layer
s	solid
Se	external shell
Se,out	external shell, side facing fire
Si	internal shell
V	vapor
0	initial condition
1	innermost reflective layer

1. Introduction

Climate change imposes the transition to clean and green renewable energy sources worldwide. In this context, hydrogen is emerging as a promising alternative energy carrier with a reduced environmental footprint [1,2]. Storage and transportation of hydrogen as a cryogenic liquid (LH_2) within specific tanks represents one of the most effective solutions to achieve a high volumetric energy density [3,4]. However, the low storage temperature of cryogenic hydrogen poses several challenges in minimizing heat transfer from the environment to avoid excessive boil-off losses.

To this purpose, thermal superinsulation materials such as perlite, hollow glass microspheres, aerogel, glass bubbles, fiber-reinforced plastic, and multilayer insulation (MLI), also combined with vacuum and active components as vapor-cooled shields or coolers, have been developed [5]. Among the most mature insulation technologies, MLI systems have the smallest volume requirement and the lowest density [6]. Thus, they represent one of the preferred choices in the transportation sector, especially on a small to medium scale, where space and weight constraints play a crucial role [7].

Despite the undoubted advantages arising from the widespread adoption of LH_2 storage and transportation technologies, several hazards must be considered due to the wide flammability range and low ignition energy of hydrogen-air mixtures [8,9]. Accidental releases may trigger dangerous events, such as flash fires [10], vapor cloud explosions [11], and jet fires [12,13], with the potential of triggering domino effects [14].

Tests by Pehr and van Wingerden et al. [15,16] involving real-scale LH_2 cryogenic tanks showed that, despite the presence of an MLI system, Boiling Liquid Expanding Vapor Explosions (BLEVEs) [17] and fireballs [18] may result from the catastrophic failure of the tank upon exposure to external fires. This was ascribed to the degradation of the insulation material. Eberwein et al. [19–21] confirmed this hypothesis experimentally, showing that high-temperature exposure can severely deteriorate MLIs (whether or not the vacuum is lost in the double wall cavity of the tank), leaving the tank unprotected from the fire heat flux. As a result, the tank pressurizes while its wall attains temperature values that induce a drop in mechanical resistance. The combination of these factors represents a significant threat to the tank integrity.

Understanding the thermodynamic response of LH_2 tanks to fire exposure is crucial to assessing and improving tank safety and supporting emergency management. Although fire tests can be considered the most robust approach to assess the behaviour of (LH_2) tanks in fire conditions and prove compliance with standards, they present several drawbacks.

Fire test campaigns are expensive and time-consuming, limiting the number of scenarios that can be considered. They also pose relevant safety and environmental issues. Ensuring test repeatability is challenging, especially in large-scale experiments. Fire test results are case-specific: the assessment of a tank with a modified design (e.g. the installation of a different insulation system and/or pressure relief device in an LH_2 tank) requires the development of specific testing procedures. Validated numerical models represent useful tools that can be used to integrate fire test results and explore tank behaviour over a wider range of conditions and scenarios. They can also be employed as a virtual workbench to assess different alternatives in the early design stages. Recently, both lumped parameters (i.e., based on a sub-division of the tank domain into zones and on the solution of heat and mass balance for each of them) and CFD (Computational Fluid Dynamics) models were developed to simulate the behaviour of tanks for the storage of cryogenic liquids (LH_2 and LNG) engulfed in fire. Examples and details of both categories of models are reported in the literature [22,23]. These models require empirical adjustments addressing the MLI effective thermal conductivity in order to match the experimental results since a systematic and robust model for the prediction of MLI performance degradation is still lacking. Thus, their application is constrained to the specific case considered. To overcome this limitation, two numerical models were recently developed and validated to simulate the heat transfer through MLI in case of deterioration induced by high temperatures. Camplese et al. [24] devoted their efforts to MLI systems based on polyester, while Hajhariri et al. and Camplese et al. [25,26] extended the approach to non-combustible MLIs. These models provide an accurate quantification of the heat flux to the tank during fire scenarios. However, they do not address the simulation of the tank response.

This study proposes an innovative approach to the safety assessment of LH_2 tanks equipped with MLI systems, based on an advanced modeling approach that integrates the high-temperature degradation of MLIs and the thermodynamic modeling of the behaviour of the fluid stored in the tank. An original lumped model was developed to simulate the tank heat-up and pressurization resulting from fire exposure. The model accounts for the action of the pressure relief valve (PRV) and includes a simplified mechanical stress analysis to investigate the possibility of tank failure. The degradation of the MLIs performances at high temperatures was simulated using the approaches proposed by Camplese et al. [24,26] and Hajhariri et al. [25].

The model was then applied to a case study that considers a typical vehicle-scale LH_2 storage tank. The response of the tank to different fire scenarios was assessed considering the categories of MLI materials most frequently applied: aluminum-based and polyester-based MLIs. The

systematic assessment and comparison of the MLI performances were carried out through the definition of specific key performance indicators (KPIs) and the identification of reference times (RTs) useful to characterize the evolution of the accident scenario.

In the following, Section 2 introduces the approach developed and the features of the MLI materials considered. Section 3 presents the model developed for MLI degradation and the KPIs defined to assess MLI performance. Section 4 introduces a case-study. In section 5 the results are presented and discussed. Section 6 draws some conclusions.

2. Overview of the approach

2.1. Phases of the study

An innovative approach was developed to assess the performance of MLI systems applied to LH_2 tanks during fire scenarios. This is based on a specific model coupled to KPIs aimed at MLI performance assessment. In order to obtain the innovative approach, the study was divided into four phases, as shown in Fig. 1.

The preliminary phase of the study was devoted to the identification and selection of the MLI systems to be considered in the study. The most popular MLIs for vehicle-scale cryogenic LH_2 storage and transportation tanks (phase 0 in Fig. 1) were selected.

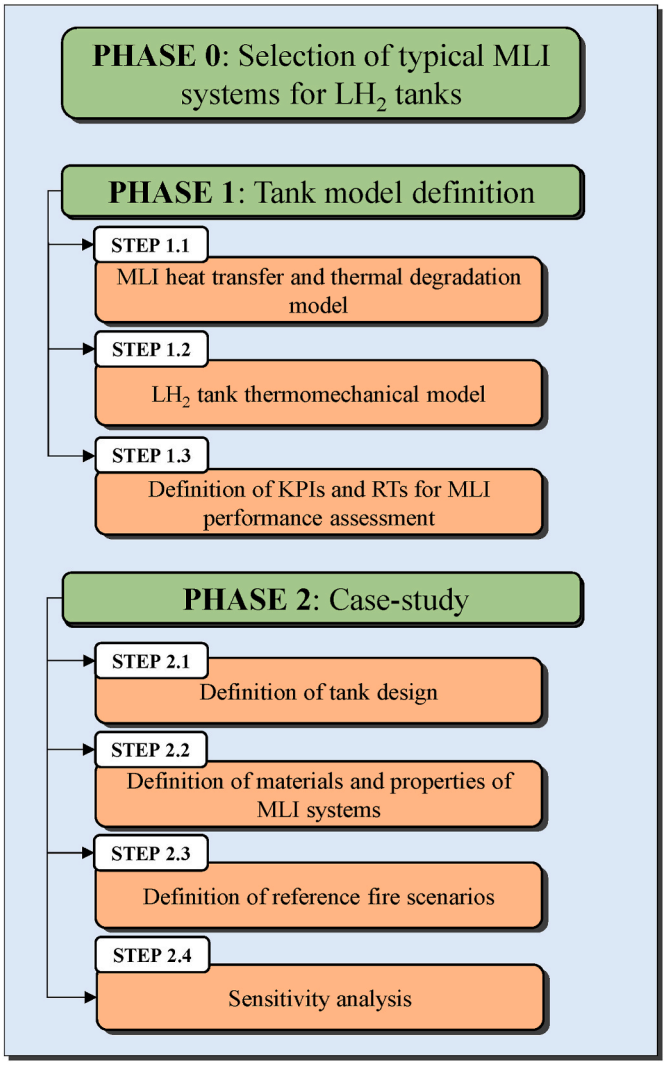

Fig. 1. Flowchart of activities.

Then, in the first phase of the study, a model for the simulation of the behaviour of LH_2 tanks in fire scenarios was developed. This was obtained as the combination of two sub-models: one that simulates the heat transfer and the thermal degradation processes in the insulation systems (Step 1.1), the other that uses a lumped approach to describe the thermomechanical response of the LH_2 tank (Step 1.2), including the hydrogen stored inside. This model calculates the pressurization and the mechanical stress in the tank shell, also taking into account the effect of the PRV action, allowing to estimate the time to failure based on a widely adopted failure criterion. A specific set of key performance indicators (KPIs) and reference times (RTs) were then defined to assess and compare the performance of MLI systems when exposed to realistic fire scenarios (Step 1.3).

In the second phase of the study, a test case was set up for the application of the performance assessment. This encompassed the identification of the constructive characteristics of a vehicle-scale LH_2 tank (Step 2.1) and its insulation system (Step 2.2), and the definition of a set of realistic fire scenarios based on a standard fire curve (Step 2.3). Finally, a sensitivity analysis was carried out to assess the effect of the variation of the values of the input parameters on the results (Step 2.4).

The following sections describe in detail each phase of the study, following the flowchart illustrated in Fig. 1.

2.2. Selection of MLI systems for LH_2 tanks

MLI systems consist of a series of thin reflective layers (typically 10 to 80 [27,28]) made of low-emissivity material, alternatively spaced by low-thermal-conductivity and high-void-fraction spacers. For cryogenic storage services, MLIs are placed within the double wall of the tank, where high-vacuum pressure conditions (around 10^{-3} Pa) are maintained [27]. This configuration minimizes the contributions of all the heat transfer mechanisms (i.e., radiation, conduction, and convection), resulting in very low heat fluxes into the tank (typically from 0.2 to 2 W/m^2 for liquid hydrogen storage [29]), and limiting boil-off (0.1–1 %/Day [30]). The most used reflective layers are pure aluminum foils and Double-Aluminized Mylar (DAM) [31]. The first ones are typically interleaved with fiberglass fleece or paper, while DAM reflective layers, which consist of a high-density polyester main core with both surfaces coated with ultra-thin aluminum, are coupled with polyester, silk, or fabric spacers. Depending on the reflective materials used, MLI systems can be grouped into two main categories: “aluminum-based” (i.e., with pure aluminum reflective layers) and “polyester-based” MLIs (i.e., with DAM reflective layers).

Over the last decades, both MLI categories were tested and adopted on large-scale (LH_2) cryogenic tanks for both static and spacecraft propellant storage purposes [32,33].

Recently issued standards, such as ISO and ADR [34,35], introduced a further distinction between “combustible” and “non-combustible” MLIs, based on the capacity of their constitutive materials to sustain or not combustion in case of ignition in oxygen-enriched atmospheres [36]. The ISO standard [34] forbids the use of “combustible” MLIs, such as polyester-based MLIs, for LH_2 applications. The ADR [35] states that this type of MLIs can be used for small tanks only. The GTR 13 [37] does not provide any limitation on this aspect. Although polyester-based MLIs may possibly be excluded from the use in the hydrogen value chain in the near future, their application will still be possible for other cryogenic fluids such as LNG.

Since the present approach aimed to provide a comprehensive overview of the performances of the most widely adopted MLIs in fire scenarios, two systems were selected for the assessment: DAM with polyester net spacer and aluminum foil reflective layer with glass fleece (see Section 4.2 for material and geometrical properties details). These are representative of the two macro categories discussed above: “polyester-based (combustible)” and “aluminum-based (non-combustible)” MLIs.

3. Model

The performance of the MLI systems considered in the present study was assessed by developing a specific model for the simulation of LH_2 tank behavior under fire exposure. This consists of the two sub-models described in the following: i) the MLI heat transfer and thermal degradation model (Section 3.1), and ii) the LH_2 tank thermomechanical model (Section 3.2).

3.1. Step 1.1: MLI heat transfer and thermal degradation model

The MLI thermal degradation model adopted in the present study is based on the approach proposed by Camplese et al. [24] for polyester-based MLIs, extended by Hajhariri et al. [25] to aluminum-based MLIs. Both approaches were validated against data from an experimental apparatus specifically designed to study the performance of MLI under fire-like conditions. Experimental data obtained by Thermogravimetric Analysis (TGA) and Differential Scanning Calorimetry (DSC) were used to characterize the relevant degradation processes. The model exploits a thermal node discretization, in which the insulation system is divided in N+2 nodes as shown in Fig. 2. A single node is assigned to each of the N reflective layers, while two additional thermal nodes are used to represent the external shell, S_e, and the internal shell S_i. A transient one-dimensional heat balance is written for each node and solved to obtain its temperature-time correlation. The heat balance equations are reported in Table 1 (Eqs. (1)–(5)) together with the other model equations. The net heat flux ($q_{rl,i}$) between nodes i and i-1 is calculated as the sum of thermal radiation (Eq. (7) of Table 1), solid conduction (Eq. (8) of Table 1), and heat transfer mechanisms in the gas phase (i.e., conduction or convection, depending on the vacuum pressure and fluid-dynamic regime: see Eqs. (9)–(15) in Table 1). As clear from Eqs. (8)–(11), the spacer properties required are only needed to calculate the heat flux terms related to spacer conduction and gas conduction/convection.

The method to calculate the heat transfer contribution of the gas ($q_{g,i}$) relies on the Sherman-Less relation for conduction and transitions to convection at high Grashof (Gr) and Rayleigh (Ra) numbers. This approach ensures the application of the model in all relevant pressure ranges, from standard operating conditions ($1.33{\cdot}10^{-4}$ to 1.33 Pa, as specified in Ref. [27]) to scenarios involving partial or complete vacuum loss, such as those observed in fire tests conducted by Wingerden et al. [16]. Further details of each contribution as well as of their physical parameters are provided elsewhere [24].

Thermal balances for the external shell and internal shell nodes require specific considerations. The heat flux terms in the external shell thermal balance (Eq. (1) in Table 1) represent the fire heat load (q_f), which is discussed in Section 3.2, and f is the heat transfer to the outermost (intact) MLI layer. The latter involves only radiation and gas heat transfer mechanisms, since a vacuum gap is usually present between these two surfaces. Eq. (5) in Table 1 is used to calculate the inner shell temperature and thus the heat flux from the inner shell to tank lading (q_{H2}). The last term is governed by the heat transfer coefficient in cryogenic fluid wetting the wall as described in Section 3.2.

Table 1
Set of equations used in the MLI heat transfer model. The symbols in the equations are defined in the nomenclature section (Eq. N°; equation number).

Node	Variable	Equation	Eq. N°
S_e	T_{S_e}	$\delta_{S_e}\rho_{S_e}c_{p,S_e}\frac{dT_{S_e}}{dt} = q_f - \frac{1}{\left(\frac{1}{\varepsilon_{S_e}}+\frac{1}{\varepsilon_N}-1\right)}\sigma\left(T_{S_e}^4 - T_N^4\right) - q_{g,Se}$	(1)
N	T_N	$\delta_{rl,N}\rho_{rl}c_{p,rl}\frac{dT_N}{dt} = q_{g,Se} + \frac{1}{\left(\frac{1}{\varepsilon_{S_e}}+\frac{1}{\varepsilon_N}-1\right)}\sigma\left(T_{S_e}^4 - T_N^4\right) - q_{rl,N}$	(2)
i	T_i	$\delta_{rl,i}\rho_{rl}c_{p,rl}\frac{dT_i}{dt} = q_{rl,i+1} - q_{rl,i}$	(3)
1	T_1	$\delta_{rl,1}\rho_{rl}c_{p,rl}\frac{dT_1}{dt} = q_{rl,2} - q_{rl,1}$	(4)
S_i	T_{S_i}	$\delta_{S_i}\rho_{S_i}c_{p,S_i}\frac{dT_{S_i}}{dt} = q_{rl,1} - q_{H2}$	(5)
–	$q_{rl,i}$	$q_{rl,i} = q_{rad,i} + q_{s,cond,i} + q_{g,i}$	(6)
–	$q_{rad,i}$	$q_{rad,i} = \frac{\sigma}{\left(\frac{1}{\varepsilon_i}+\frac{1}{\varepsilon_{i-1}}-1\right)}\left(T_i^4 - T_{i-1}^4\right)$	(7)
–	$q_{s,cond,i}$	$q_{s,cond,i} = \frac{f_i^2 k_s}{D_x}\left(T_i - T_{i-1}\right)$	(8)
–	$q_{g,i}$	$q_{g,i} = \begin{cases} q_{g,cond,i} & \text{if } Gr < 2860 \\ q_{g,conv,i} & \text{if } Gr \geq 2860 \end{cases}$	(9)
–	Gr	$Gr = \frac{g\alpha\Delta T D_x^3}{\nu^2}$	(10)
–	$q_{g,cond,i}$	$q_{g,cond,i} = \left[\frac{D_x}{k_g} + \frac{2-\theta}{\theta}\cdot\frac{\sqrt{\frac{\pi M\bar{T}}{2R}}}{\left(1+\frac{\zeta}{4}\right)P_r}\right]^{-1}\left(T_i - T_{i-1}\right)$	(11)
–	$q_{g,conv,i}$	$q_{g,conv,i} = Nu\frac{k_g}{D_x}\left(T_i - T_{i-1}\right)$	(12)
–	Nu	$\begin{cases} Nu = 0.197 Ra^{1/4}\left(\frac{\delta}{H}\right)^{1/9}, 2\times10^3 < Ra < 2\times10^5 \\ Nu = 0.073 Ra^{1/3}\left(\frac{\delta}{H}\right)^{1/9}, 2\times10^5 < Ra < 1.1\times10^7 \end{cases}$	(13)
–	Ra	$Ra = Gr{\cdot}Pr$	(14)
–	Pr	$Pr = \frac{\mu c_{p,g}}{k_g}$	(15)

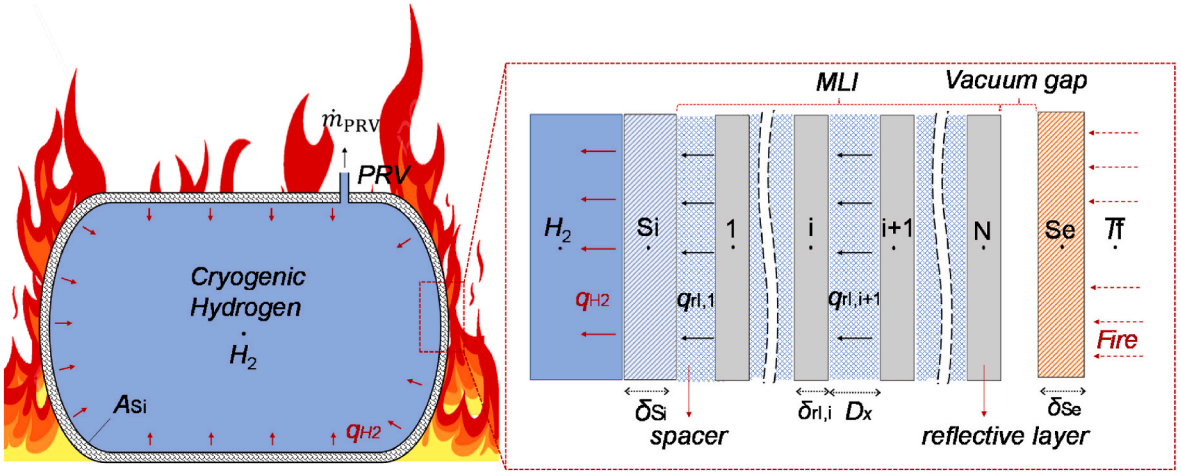

Fig. 2. Schematic representation of the thermal node discretization adopted to describe the heat transfer problem. Se = external shell, Si = internal shell. Nodes 1 to N refer to the MLI radiative layers.

Table 2
Degradation kinetics of the two types of MLI addressed in the study. The symbols in the equations are defined in the nomenclature section. The equation numbers are reported in the third and fifth column of the table respectively for polyester-based and Aluminum-based MLIs.

Variable	Polyester-based MLI	Eq. N°	Aluminum-based MLI	Eq. N°
f_i	$f_i = f_0 \cdot Y_{s,i}$	(16)	$f_i = f_0$	(20)
$\delta_{rl,i}$	$\delta_{rl,i} = \delta_{rl,0} \cdot Y_{s,i}$	(17)	$\delta_{rl,i} = \delta_{rl,0}$	(21)
$Y_{s,i}$	$\begin{cases} Y_{s,i} = m_{s,i}/m_{s,0} \\ \frac{dY_{s,i}}{dt} = -A\, exp\left(-\frac{E_a}{RT_i}\right) Y_{s,i}{}^n \end{cases}$	(18) (19)	$Y_{s,i} = 1$	(22)
Degradation criterion	$Y_{s,i} = 0.16$	–	$T_i = 660.3\ ^\circ C$	–

In order to take into account the possible high-temperature degradation of MLI materials, two distinct approaches are used, depending on the MLI type considered. The associated sets of equations are reported in Table 2.

In the case of polyester-based MLI, both the relative density of the i-th spacer (f_i) and the layer thickness ($\delta_{rl,i}$) vary as a function of the solid material mass loss (Eqs. (16) and (17) in Table 2), according to the approach proposed by Camplese et al. [24]. The terms f_0 and $\delta_{rl,0}$ represent the initial nominal values of f_i and $\delta_{rl,i}$, respectively. The sample residual fraction, $Y_{s,i}$, is defined by Eq. (18) in Table 2 and represents the residual mass of the i-th layer ($m_{s,i}$) normalized to its initial value ($m_{s,0}$). This is calculated at each time step by solving the kinetic model of Eq. (19) in Table 2 for each reflective layer. n, A and E_a represent the apparent order of reaction, pre-exponential factor, and activation energy respectively, which were estimated from thermogravimetric analysis [24]. Factors f_i and $\delta_{rl,i}$ are updated at each time step until degradation threshold $Y_{s,T}$ (i.e., the value of the residual mass fraction, Y_s, at which the radiative layer is considered to be destroyed; $Y_{s,T} = 0.16$, is reached [24]. Then, both the i-th reflective layer and the i-th spacer are assumed to be destroyed and removed from the simulation. This approach allows to simulate a gradual degradation of both the reflective layer and spacer material.

In the case of aluminum-based MLI, the complete deterioration of each reflective layer is assumed to occur instantaneously when its temperature reaches the melting point of aluminum (933.5 K [38]). At this temperature, fiberglass spacers typically used in these types of MLI may remain intact in place, maintaining their original configuration, even in case of complete degradation of the reflective layers [25]. Hajhariri et al. [25] highlighted that the spacer may absorb a fraction of the incident heat radiation, but a reliable correlation for its quantification is still missing. Therefore, in the present model, in order to obtain conservative results, the i-th spacer layer of aluminum-based MLI is removed instantaneously when the i-th reflective layer fails, neglecting the limited shielding effect provided by the spacer. Before the degradation takes place, the properties of both the i-th reflective layer and the i-th spacer are assumed as constant and equal to their initial nominal values (see Eqs (20) and (21) in Table 2), as suggested in previous studies [25,26].

3.2. Step 1.2: LH_2 tank thermomechanical model

A single-zone lumped equilibrium model is used to simulate the pressurization inside the tank. The fluid domain is schematized with one thermal node (H_2; see Fig. 2) for which mass and thermal balances are defined assuming a uniform temperature, T_{H2}, and thermodynamic equilibrium between the liquid and gaseous hydrogen phases (see Eqs. 23 and 24 in Table 3), thus neglecting the effect of thermal stratification. Studies addressing tanks under fire exposure show that this assumption is reasonable for small-sized tanks [39,40] as the one analysed in the present study. In the case of larger tanks, experimental evidence shows that thermal stratification ends after the PRV opening [41,42]. Both balance equations consider the action of the pressure relief valve (PRV) through the activation factor ϕ, which is 0 when the valve is closed and 1 when is open, and the outlet mass flow term $\dot{m}_{PRV}$. This is calculated using Eq. 27 [43], assuming a vapor fraction of 1 for the outlet stream. The specific enthalpy of the PRV outlet is calculated according to this assumption. The PRV cross-sectional area (A_{PRV}) and its opening and closing set point pressures ($P_{PRV,open}$ and $P_{PRV,close}$) derive from the PRV sizing criteria. The values assumed in the case-study are reported in Section 4.1.

The term q_{H2} in the energy balance (Eq. (24) in Table 3) represents the heat flux from the inner shell and is calculated according to Eq. (29) (Table 3), where A_{Si}, T_{Si}, and h are the inner shell surface, inner shell

Table 3
Set of equations used in the tank pressurization model. The symbols in the equations are defined in the nomenclature section (Eq. N°; equation number).

Node	Variable	Equation	Eq. N°
H_2	m_{H2}	$\frac{dm_{H2}}{dt} = -\phi \dot{m}_{PRV}$	(23)
H_2	$\widehat{U}_{H2}$	$\frac{d(m_{H2}\widehat{U}_{H2})}{dt} = q_{H2}A_{Si} - \phi \dot{m}_{PRV}\widehat{H}_{PRV}$	(24)
H_2	P^a	$P = f(\rho_{H2}, \widehat{U}_{H2})$	(25)
-	ϕ^b	$\phi = \begin{cases} 0, PRV\ close \\ 1, PRV\ open \end{cases}$	(26)
-	$\dot{m}_{PRV}{}^c$	$\dot{m}_{PRV} = \begin{cases} K_d A_{PRV}\sqrt{\gamma\rho P\left(\frac{2}{\gamma+1}\right)^{\left(\frac{\gamma+1}{\gamma-1}\right)}}, \frac{P_o}{P} \le \left(\frac{2}{\gamma+1}\right)^{\left(\frac{\gamma}{\gamma-1}\right)} \\ K_d K_b A_{PRV}\sqrt{\gamma\rho P\left(\frac{2}{\gamma+1}\right)^{\left(\frac{\gamma+1}{\gamma-1}\right)}}, \frac{P_o}{P} > \left(\frac{2}{\gamma+1}\right)^{\left(\frac{\gamma}{\gamma-1}\right)} \end{cases}$	(27)
-	K_b	$K_b = \sqrt{\frac{\left(\frac{2}{\gamma-1}\right)\left[\left(\frac{P_o}{P}\right)^{2/\gamma} - \left(\frac{P_o}{P}\right)^{(\gamma+1)/\gamma}\right]}{\left(\frac{2}{\gamma+1}\right)^{(\gamma+1)/(\gamma-1)}}}$	(28)
-	q_{H2}	$q_{H2} = h(T_{Si} - T_{H2})$	(29)
-	h	$h = (h_L A_L + h_V A_V)/A_{Si}$	(30)

a The equation of state is solved through the "Coolprop" tool. Further details are reported elshewhere [42,43].
b the valve remains closed until the pressure reaches $P_{PRV,\ open}$, and it remains so until the pressure below $P_{PRV,\ close}$.
c K_d is the discharge coefficient of the PRV and is assumed equal to 0.82 [46].

temperature, and the heat transfer coefficient of the fluid in contact with the wall. The heat transfer coefficient is obtained by Eq. (30) (Table 3) as the weighted sum of the liquid and vapor coefficients (namely, h_L and h_V) considering the tank surface areas wetted by the liquid and the vapor phases respectively (namely, A_L and A_V). h_L was calculated according to Wang et al. [44] which suggested a set of correlations to estimate the heat transfer coefficient between the tank wall and the LH_2 for each region of the boiling curve. h_V was calculated through the equations proposed by Churchill and Usagi [45].

At each timestep, the mass and energy balances for the LH_2 tank are solved to find the specific internal energy ($\widehat{U}_{H2}$) and the mass of hydrogen lading (m_{H2}). The other thermodynamic properties of the hydrogen phases are obtained from the "Coolprop" database [47], assuming thermodynamic equilibrium between liquid and vapor phases (until both are present inside the tank, as in the case-study considered). Fluids properties in "Coolprop" are based on Helmholtz energy formulation and on the equation of state specifically developed for hydrogen by Leachman et al. [48] which requires two independent variables as input parameters. In the proposed model, the pressure of hydrogen inside the tank, P, is calculated by the "Coolprop" tool using $\widehat{U}_{H2}$, and the hydrogen density, ρ_{H2}, (directly obtained from m_{H2} and the tank volume V_{Si}) are used as input parameters (see Eq. (25) in Table 3).

On the one hand, it is important to remark that the lumped model proposed neglects the effect of thermal stratification, which is known to speed up tank pressurization [49]. Although several multi-zone models that account for this phenomenon have been proposed in the last decades, all rely on adjustable parameters fine-tuned to match the results of specific sets of experimental data (which depend on tank geometry and operating conditions). On the other hand, the advantage of CFD models, not needing the use of such adjustable parameters comes at a high computational cost, which hinders their use for systematic studies that require a high number of simulations.

Since the focus of the present study is the systematic comparative assessment of MLI performances in fire scenarios rather than on detailed thermo-fluid dynamic analysis of the hydrogen behaviour in the tank exposed to the fire, also considering that the thermal stratification tends to vanish as a result of boiling-induced mixing caused by the opening of the PRV [50], the single-node equilibrium modeling approach described above was considered the most suitable for the purpose. This is in line with the methodology proposed by ISO 21014:2019 for the determination of the performance of cryogenic insulation [51]. The current literature lacks sufficiently detailed experimental data concerning LH_2 tanks featuring MLI systems under fire exposure. For instance, in the real-scale fire tests reported by Pehr [15] and van Wingerden et al. [16], details on the insulation system used were not provided. Furthermore, in part of the tests, the fire engulfment was not uniform and varied considerably over the duration of the experimental run, making the resulting measurements unsuitable for validation purposes. Therefore, following the approach of several previous studies on hydrogen tanks [52,53], the validation process for the pressurization submodel was based on experimental data on the self-pressurization of a liquid nitrogen tank, that were considered the best available data to provide at least a preliminary model validation.

The possibility of inner tank failure due to mechanical stresses is evaluated in the model by applying the Von Mises yield (maximum distortion energy) criterion. In particular, in order to assess the integrity of the tank at each timestep, it is assumed that the failure of the inner vessel occurs when the equivalent mechanical stress induced by pressure build-up (σ_V) equals the yield strength of the shell material (σ_y), as described by Eq. (31).

$$\sigma_V = \sigma_y \tag{31}$$

The first term (σ_V) is obtained by Eqs. (32)–(35), where σ_l, σ_h, and σ_r are the longitudinal, circumferential, and radial primary stresses, calculated according to the thin-wall assumption [54], r and δ_{Si} represent the inner shell radius and thickness, and P_g is the inner tank gauge pressure.

$$\sigma_V = \sqrt{\frac{(\sigma_l - \sigma_h)^2 + (\sigma_h - \sigma_r)^2 + (\sigma_l - \sigma_r)^2}{2}} \tag{32}$$

$$\sigma_l = \frac{P_g \cdot r}{2\delta_{Si}} \tag{33}$$

$$\sigma_h = \frac{P_g \cdot r}{\delta_{Si}} \tag{34}$$

$$\sigma_r = -P_g \tag{35}$$

The yield strength of the shell material (σ_y) is calculated at each timestep accounting for the effect of temperature according to the strength reduction coefficients provided by the standard [55]. The maximum inner shell temperature ($T_{Si,max}$) is estimated using Eq. (36), which is derived from Eq. (5) eliminating the heat transferred from the shell to the fluid in the tank (i.e. $q_{H2} = 0$)

$$\delta_{Si}\rho_{Si}c_{p,Si}\frac{dT_{S_i,max}}{dt} = q_{rl,1} \tag{36}$$

This assumption allows obtaining a conservative estimation of the shell temperature, avoiding introducing uncertainties related to the value of the heat transfer coefficient.

The fire boundary condition is defined assuming a full engulfment scenario, modeled as indicated by ISO 21843 [56]. The heat flux entering the external wall of the thank, q_f, is computed at each time step according to Eqs. (37)–(39), where $q_{rad,f}$ and $q_{conv,f}$ represent the fire radiative and convective heat fluxes, ε_f is the flame emissivity (here assumed equal to 1), T_f and T_{Se} are the flame and external shell temperatures, $\varepsilon_{Se,out}$ is the emissivity of the external wall on the side facing the fire, and h_f is the fire convective heat transfer coefficient (here set to 10 W/(m^2·K).

$$q_f = q_{rad,f} + q_{conv,f} \tag{37}$$

$$q_{rad,f} = \sigma\varepsilon_{Se,out}\left(\varepsilon_f T_f^{\,4} - T_{Se}^{\,4}\right) \tag{38}$$

$$q_{conv,f} = h_f\left(T_f - T_{Se}\right) \tag{39}$$

Before each simulation run, the steady-state temperature profile obtained with $T_{Se} = 293$ K and a fluid hydrogen temperature, T_{H2}, of 20 K (corresponding to the saturation temperature of hydrogen at atmospheric pressure [38]) are set as the initial conditions through the tank and MLI system. It should be considered that, as discussed in the following, the actual operating temperature is between 20 and 26 K, where the latter value is the saturation temperature corresponding to $P_{PRV,open}$ (see Table 4). At each timestep, mass and thermal balances considered in both MLI degradation and tank pressurization models are solved iteratively using a fully implicit discretization scheme [57] up to the point where the highest (among all nodes) relative deviation of the temperature calculated at two consecutive iterations drops below 10^{-7}.

3.3. Step 1.3: Performance assessment of MLI systems under fire exposure

The performance and the resistance of MLI systems play a key role in determining whether or not a cryogenic tank can withstand fire exposure. The capacity of protection against the external heat load is strongly affected by the rate and extent of deterioration of the material at high temperatures [20].

The numerical model presented above calculates the dynamic evolution of several parameters, such as the temperature and the heat flux through the insulation system and the tank walls, the extent of the degradation of each MLI layer, the pressurization rate, and the high-temperature weakening of the steel structure. These are all elemental

Table 4
Tank features and material properties.

Section	Parameter	Symbol	Value	Unit of measure	Source
Internal tank	Length	L	0.72	m	–
	Diameter	D	0.46	m	–
	Volume	V_{Si}	0.12	m^3	–
	Inner tank surface	A_{Si}	1.34	m^2	–
	Wall thickness	δ_{Si}	0.002	m	–
	Wall density	ρ_{Si}	7944	kg/m^3	[58]
	Wall heat capacity	$c_{p,Si}$	500	J/(kg·K)	[58]
	Wall thermal conductivity	k_{Si}	15	W/(m·K)	[58]
	Internal wall emissivity	ε_{Si}[c]	1	–	[19]
	Yield strength	σ_y	$\sigma_{y,293K}$[a]·$k_y(T_{Si,max})$[b]	MPa	[55,59]
	PRV opening section	A_{PRV}	$5.11{\cdot}10^{-4}$	m^2	[46]
	PRV opening pressure	$P_{PRV,\ open}$	0.47	MPa	[15]
	PRV closing pressure	$P_{PRV,\ close}$	0.47	MPa	[60]
External tank	Wall thickness	δ_{Se}	0.002	m	–
	Vacuum gap thickness	Δx	0.035	m	[15]
	Wall density	ρ_{Se}	7944	kg/m^3	[58]
	Wall heat capacity	$c_{p,Se}$	500	J/(kg·K)	[58]
	Wall thermal conductivity	k_{Se}	15	W/(m·K)	[58]
	Wall emissivity (side facing the fire)	$\varepsilon_{Se,out}$	0.5	–	[24]
	Wall emissivity (side facing the inner tank wall)	ε_{Se}[c]	0.44	–	[19]

[a] $\sigma_{y,293K}$ is the yield strength at 293 K and was considered equal to 240 MPa [59].
[b] $k_y(T_{Si,max})$ is the reduction factor (relative to the yield strength) and varies between 1 and 0 within 293 and 1473 K, according to EN 1993-1-2:2024 for the steel type considered [55].
[c] The experimental values are reported from Eberwein et al. [19] and derived from a test involving a polyester-based MLI system at a maximum temperature of 1023 K.

aspects needed to investigate in detail the tank response to external fire. Many other studies proposed Key Performance Indicators (KPIs) to summarize the information obtained from complex modelling approaches and to identify hazardous operating regions, thus supporting the improvement of storage safety and emergency management in fire scenarios [61]. Following this rationale, a set of KPIs and reference times were identified to assess and compare MLI systems based on a systematic approach.

Two KPIs were introduced to quantify the insulation performance of MLIs during and after fire exposure: the Degradation Index for Fire conditions (*DIF*) and the Degradation Index for Post-fire exposure conditions (*DIP*). These are based on the concept of effective thermal conductivity (k_{eff}), calculated by Eq. (39). This parameter is used in many standards and regulations [31,36,62] to quantify and compare the MLI insulation performances and can be directly linked to the heat leaking into the tank either in normal operating conditions and in fire conditions (see Eq. (39)). Therefore, monitoring the extent of k_{eff} variation with respect to initial or normal operating conditions allows for a quantitative evaluation of performance deterioration under fire attack.

Based on these principles, the *DIF* is defined as the ratio between the instantaneous effective thermal conductivity of the MLI system during fire exposure, $k_{eff,F}$, and $k_{eff,Std}$, the effective thermal conductivity obtained in steady-state normal operating conditions (tank inner temperature of 20 K and an ambient temperature of 293 K) calculated using Eq. (41). This indicator provides a measure of the system performance deterioration during fire exposure: a higher *DIF* corresponds to higher heat fluxes into the tank and, as a consequence, to an accelerated pressurization and temperature increase in the wall, inducing structural weakening and thus increasing the risk of failure before fire suppression.

The second KPI introduced, *DIP*, quantifies the loss of insulation performance after the fire is extinguished, providing an indication of how fast the tank will be prone to self-pressurize in the aftermath of the fire, thus supporting the post-fire emergency management. This is defined by Eq. (42), where the $k_{eff,P}$ represents the effective thermal conductivity at normal operating conditions after the fire exposure (tank inner temperature of 20 K and ambient temperature of 293 K).

$$k_{eff} = \frac{q_{rl,1} \cdot \Delta x}{(T_{Se} - T_{Si})} \tag{40}$$

$$DIF = \frac{k_{eff,F}}{k_{eff,std}} \tag{41}$$

$$DIP = \frac{k_{eff,P}}{k_{eff,std}} \tag{42}$$

Besides the KPIs that quantify the performance of the insulation, a set of Reference Times (RTs) was defined, considering key events that indicate to what extent the integrity of the tank can be threatened by a given fire scenario. Four RTs corresponding to key events during fire exposure were identified.

i. the onset of degradation time (t_{od}), defined as the time taken by the outermost reflective layer to reach 99 % of the total weight loss for polyester-based MLI or 99 % of the degradation temperature for aluminum-based MLI (i.e., 923 K);
ii. the total degradation time(t_{td}), defined as the time it takes for the entire MLI system to completely degrade;
iii. the time of the first PRV opening (t_{PRV});
iv. the time to failure (*ttf*), calculated as described in Section 3.2.

4. Case-study

The model developed was applied to test and compare the performances of polyester and aluminum-based MLIs, simulating the behavior of a vehicle-scale double-walled tank filled with liquid hydrogen under realistic fire conditions. In the following sections, the tank design (see Section 4.1), MLI systems properties (see Section 4.2), and the reference fire scenarios (see Section 4.3) considered in the case-study are presented.

4.1. Step 2.1: Tank design features

The LH_2 tank considered in this study is a double-walled horizontal cylindrical tank with two elliptical ends. The geometrical characteristics of the tank were derived from standards for cryogenic tanks for vehicle application [34,46,60]. The inner tank has a length of 2.1 m and a diameter of 0.55 m. By approximating the tank surface to a cylinder, the resulting inner volume, V_{Si}, and internal surface area, A_{Si}, are 0.5 m^3 and

4.1 m^2, respectively. The thickness of the gap between the internal and external walls is equal to 0.035 m. These dimensions are representative of LH_2-powered heavy-duty vehicles [7].

The tank is designed to operate at atmospheric pressure and is equipped with a pressure relief valve (PRV). The liquid hydrogen temperature was assumed equal to the saturation temperature at atmospheric pressure (20 K). The maximum allowable working pressure (MAWP) was set to $3.9{\cdot}10^5$ Pa as in the LH_2 tank used in the fire test by Pehr [15]. The corresponding range of the liquid hydrogen temperature (20–26 K) has a negligible effect on modelling results.

The opening and closing set point pressures ($P_{PRV,open}$ and $P_{PRV,close}$) were calculated according to the ISO 13985:2006 [34] as the 121 % of the MAWP ($4.7{\cdot}10^5$ Pa) and the 90 % of $P_{PRV,open}$ ($4.2{\cdot}10^5$ Pa), respectively.

The PRV opening section (A_{PRV}) was sized through the ISO 21013–3:2016 [46], assuming the worst-case scenario among those proposed by the standard: tank under fire conditions with loss of vacuum with air or nitrogen. This resulted in a circular discharging section of $1.4{\cdot}10^{-3}$ m^2.

AISI 316L (i.e., austenitic steel number 1.4404 according to EN 10027–2:2015 [63]) was assumed as the material of the tank shell, as particularly suitable for cryogenic applications [64]. The yield strength (σ_y) was calculated at each timestep during the simulation by scaling the reference value at 293 K (i.e., 240 MPa; [59]) by a reducing factor (k_y) that depends on the temperature according to EN 1993-1-2:2024 [55]. The inner and outer shell thicknesses (namely, δ_{Si} and δ_{Se}) were both set to 0.002 m, upon verification of compliance with the minimum requirements imposed by regulations (Annex E of ISO 21009–1:2022 [60]). The other material properties required for model equations are listed in Table 4.

In the present study, it is assumed that 50 % of the inner tank volume is occupied by liquid hydrogen in equilibrium with its vapor according to the fire test performed by Pehr [15] on a vehicle-scale liquid hydrogen tank. Simulations considering a higher fill level (80 %, corresponding to the minimum filling level according to CGA H-3 standard) were also carried out, the results of which are reported in the Supplementary Material (see Section S.C of the Supplementary Material).

4.2. Step 2.2: Definition of materials and properties of MLI systems

Two different MLI systems were considered in the case-study. These were selected to be representative of the two main types of materials identified in Section 2.2. The first is aluminum-based and consists of pure aluminum reflective foils and fiberglass fleece spacers. The second is polyester-based with DAM reflective layers and polyester (Dacron net) spacers. The properties of the two MLI materials are summarized in Table 5 and have been selected according to previous studies [24,25], where the specific assumptions and the sources of the values assumed for the properties of the materials are listed.

The insulation systems are applied within the vacuum gap between the double walls of the tank, with the inner wall in direct contact with the first spacer layer, while the last (outermost one) reflective layer is separated from the external wall by a vacuum gap. For both MLI systems, 80 layers are selected as those used in the vehicle-scale LH_2 tanks [66]. According to previous studies [24], the pressure in the vacuum gap was considered equal to 10^{-3} Pa and was assumed constant throughout the simulation, disregarding the possible loss of vacuum.

4.3. Step 2.3: Definition of reference fire scenarios

Fire scenarios involving LH_2 tanks can vary from local to full engulfment modes. While, especially for large tanks, the first type of scenario is often more representative of a real accident [67], when considering transport accidents involving small tanks, full engulfment is representative of conditions that occurred in several past accidents. Thus, full engulfment is widely used as the reference scenario in fire test standards and regulations [56,68]. Indeed, this was the target fire condition for the LH_2 tank fire tests available in the literature [15,16]. Therefore, full engulfment conditions were assumed in the present study.

The dynamic evolution of the heat flux on the tank outer wall is obtained from Eqs. (37)–(39) (see Section 3.2), in which the flame temperature (T_f) may be obtained from fire safety standards [69–72]. The flame temperature vs time curve reported in EN 1363–2:1999 [70] to represent a typical hydrocarbon pool fire is taken as a reference in the present study. This is described by Eq. (43). When the coefficient ψ_f is equal to 1, Eq. (43) corresponds to the EN 1363–2:1999 standard curve [70]. The coefficient ψ_f was introduced in the present assessment to explore a wide range of fire intensities without varying the fire growth dynamic of the reference curve. A total of 8 simulations were performed for each MLI type, varying ψ_f between 0.3 and 1 with a step of 0.1. The resulting flame temperature curves are presented in Fig. 3.

$$T_f = 1080 \cdot \psi_f\left(1 - 0.325e^{-0.167t} - 0.675e^{2.5t}\right) + 293.15 \quad (43)$$

4.4. Step 2.4: Sensitivity analysis

The tank geometry and the insulation properties considered for the case study (see Sections 4.1 and 4.2) are representative of the state-of-the-art solutions adopted in LH_2-fuelled vehicles. Nevertheless, the input parameters may vary when different applications are considered. Actually, the specific target boil-off rates adopted in different application require different insulation performances. This reflects on potential differences affecting: i) the number of MLI reflective layers [51]; ii) the space and weight constraints affecting the insulation gap thickness between the space available for insulation [7]; iii) the MLI installation methods, determining the layer density [27]; and iv) the specific application, that may orient the selection of different MLI materials

Table 5
Materials properties of the MLI systems considered in the case-study.

Component	Property	Symbol	Polyester-based MLI[a]	Aluminum-based MLI[b]	Unit
Reflective layer	Material	–	**Double-Aluminizad Mylar (DAM)**	**Pure aluminum**	
	Layers number	N	80	80	–
	Thickness	$\delta_{rl,0}$	$1.2{\cdot}10^{-5}$	$9{\cdot}10^{-6}$	m
	Specific heat capacity	$c_{p,rl}$	1000	950	J/(kg·K)
	Density	ρ_{rl}	1380	2700	kg/m^3
	Emissivity	ε_i	0.04	$7.2{\cdot}10^{-5}{\cdot}T_i{+}3.2{\cdot}10^{-3}$[c]	–
Spacer	Material	–	**Dacron net**	**Fiberglass fleece**	–
	Relative density of the spacer to the solid material	f_0	0.0358	0.0164	–
	Spacer thickness	D_x	$2.88{\cdot}10^{-4}$	$3.66{\cdot}10^{-4}$	m
	Thermal conductivity of the solid spacer material	k_s	0.195	0.8	W/(m·K)

[a] from Camplese et al. [24], also reporting the sources of material physical properties.
[b] from Hajhariri et al. [25], also reporting the sources of material physical properties.
[c] The emissivity is expressed according to Ref. [65] correlation, where T_i is the temperature of the ith reflective layer.

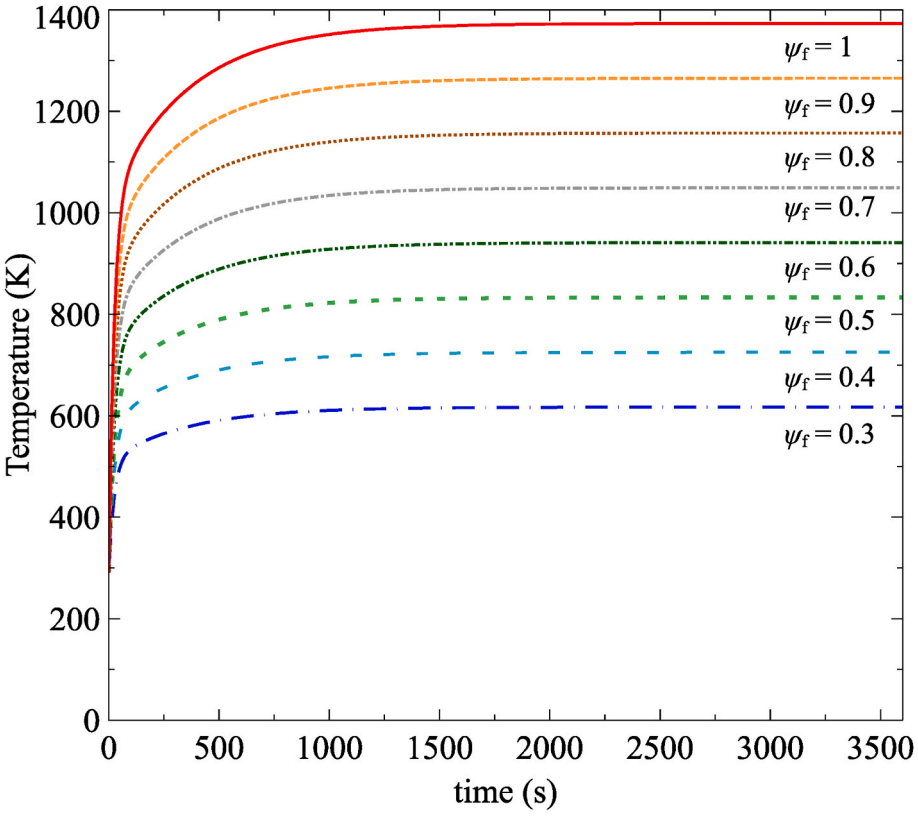

Fig. 3. Fire scenarios considered in the present study: flame temperature vs time curves for different flame intensity factors (ψ_f).

Table 6
List of parameters considered in the sensitivity analysis.

Empirical fluid dynamic and heat transfer parameters	
h	Hydrogen convective heat transfer coefficients
K_{dr}	PRV discharge coefficient
Parameters of the insulation system	
N	Number of MLI reflective layers
ε_{rl}	Surface emissivity of the reflective layer
ε_{Si}	Surface emissivity of the inner tank wall
ε_{Se}	Surface emissivity of the outer tank wall (side facing the MLI)
k_s	Thermal conductivity of the spacer material
f	Relative density of the spacer to the solid spacer material
D_x	Spacer thickness
P_r	Vacuum pressure within the insulation system
Tank operating parameters	
Δx	Vacuum gap thickness between the double walls of the tank
P_0	Initial pressure of stored liquid hydrogen

[35]. Therefore, a sensitivity analysis was performed to assess the influence of the selected model parameters on the model results. The analysis is aimed at assessing the robustness of the model and at providing a detailed insight concerning the uncertainty associated with parameter selection. The parameters are grouped in three main categories: empirical fluid dynamic and heat transfer parameters, parameters of the insulation system, and tank operating parameters, as listed in Table 6.

The sensitivity analysis was performed systematically varying each of the selected parameters of ±10 % with respect to the reference value reported in Section 4.1 or 4.2. The results are presented in Section S.D of the Supplementary Material.

Table 7
Comparison of the values of the reference times (see section 3.3) obtained for polyester-based MLI and aluminum-based MLI considering the most severe fire curve ($\psi_f = 1$). The relative increase of reference times for aluminum-based MLIs with respect to polyester-based MLIs is also calculated.

RT	unit	Polyester-based MLI	Aluminum-based MLI	Relative increase
t_{od}	s	126	174	38 %
t_{td}	s	396	528	33 %
t_{PRV}	s	402	534	33 %
ttf	s	714	798	12 %

5. Results and discussions

5.1. Results of case-study

Fig. 4 reports the pressure build-up, the flame temperature, and the maximum internal shell temperatures evolution calculated in the case-study for the LH_2 tank equipped with Aluminium-based (Fig. 4a–c, and e) and Polyester-based (Fig. 4b–d, and f) MLI under three different fire scenarios, corresponding to $\psi_f = 1$, 0.7, and 0.5. Details on the other parameters, such as the MLI layer temperature, the heat flux into the inner tank wall and liquid hydrogen mass variation over time are reported in the Supplementary Material, together with the results obtained considering alternative fire curves.

In the first period of fire exposure, the duration of which varies with the fire intensity and the material deterioration of MLI, the tank pressure and the inner tank maximum temperature remain close to their initial values despite the fast growth in the fire curve.

Focusing on the most severe fire curve ($\psi_f = 1$, see Fig. 4a and b), it is possible to observe that this initial phase extends beyond the onset of degradation (t_{od}). Then, a sudden increase in both pressure and temperature is registered, which occurs immediately after the time at which the total degradation of the MLI system (t_{td}) is reached, leading to the

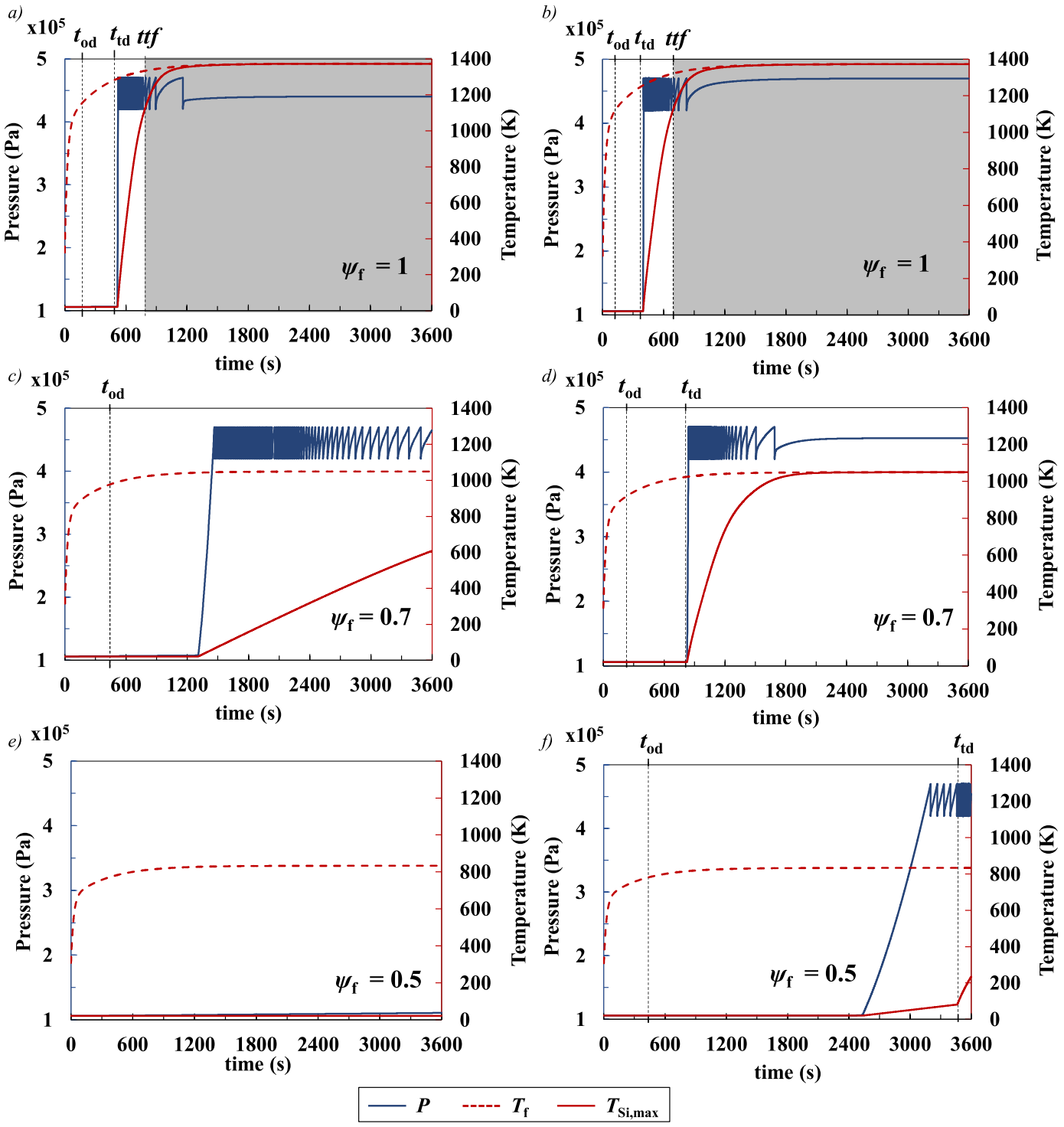

Fig. 4. Pressure (blue line), flame (dashed red line), and maximum inner shell (continuous red line) temperature history obtained for the case study considering different values of ψ_f. Panels (a), (c), and (e) refer to Aluminum-based MLI, while (b), (d), and (f) refer to polyester-based MLI. The values calculated for the reference times t_{od}, t_{td}, and ttf (see Section 3.3) are also reported. Results in the shaded region refer to simulation times higher than the ttf and are reported for the sake of completeness. (For interpretation of the references to colour in this figure legend, the reader is referred to the Web version of this article.)

activation of the PRV. After several PRV opening and closing cycles, the tank fails (i.e. the *ttf* is reached) due to the decrease in its mechanical strength, caused by the high temperature of the inner shell (see Section 3.2). The results in Fig. 4a and b shows that aluminum-based MLI has a higher resistance to fire exposure as compared to polyester-based MLI, providing a longer protection to the tank. This is reflected in the values of the reference times defined in section 3.3 and reported in Table 7: for the most severe fire curve.

When milder fire conditions are considered, a delay in the pressurization and in the increase of the inner shell temperature is recorded. For $\psi_f = 0.7$ (Fig. 4c and d), the tank survives the 3600 s fire exposure regardless of the MLI material considered. However, while the polyester-based MLI is totally degraded after less than 840 s (14 min), part of the aluminum-based one (1 layer in this specific case) remains in place,

resulting in a delayed and slower increase of the pressure and the inner shell temperature. Finally, when the fire intensity is further decreased ($\psi_f = 0.5$, see Fig. 4e and f), the aluminum-based system shows no sign of degradation, providing effective protection to the tank (the pressure and inner shell temperature increase is negligible). On the contrary, the polyester-based MLI undergoes a slow, yet complete degradation, which causes the tank to pressurize up to the PRV opening set point. The pressurization rate varies considerably, depending on both the insulation type and the fire intensity. This variability reflects the values of the heat flux to the inner tank calculated for the case studies and reported in the Supplementary Material (see Figure B4 in Section S.B of the Supplementary Material). The pressure increase obtained in the most severe fire conditions is compatible with the measurements from fire tests on aluminum MLI-insulated liquid hydrogen tanks with a size similar to that considered in the present study. In the test by Pehr [15], where the maximum fire temperature was approximately 1200 K (thus in line with the fire intensity when $0.8 \leq \psi_f \leq 0.9$), the pressure increases from atmospheric to the PRV opening set point (i.e., 0.47 MPa as in the present study) in around 180 s. In a test featuring milder fire conditions (average fire temperature of 1140 K, with the flame engulfment mainly limited to the lower half of the tank) Van Wingerden et al. [16] measured an average pressurization rate of 1500 Pa/s, with peaks of 3300 Pa/s, compatible with the 2000 Pa/s and 3300 Pa/s obtained in the case where $\psi_f = 0.7$ and 0.8, respectively. It is worth remarking that the EN 1363–2:1999 standard curve (i.e., for $\psi_f = 1$) results in a fire load that is more severe than that applied in any aluminum MLI insulated liquid hydrogen tank fire test reported in the literature to date (no test on polyester MLI insulated tanks is publicly available). Thus, the relevant results, including the very fast pressurization illustrated in Fig. 4a and b, can be considered as a worst-case scenario. Further details are reported in the Supplementary Material.

Overall, the specific results shown in Fig. 4 provide a detailed insight into the tank and MLI system response to fire exposure, which can be summarized as follows.

- The insulation system prevents the increase of tank pressure and shell temperature for a lag time that depends on the severity of the fire and the MLI material;
- When the integrity of the MLI system is fully preserved, the tank can survive prolonged fire exposure (see Fig. 4c);
- In case of partial degradation, the MLI system is still able to delay and slow down pressurization to the point that, if the PRV sizing is appropriate, the tank failure can be avoided.

These are key aspects to be regarded in the emergency response planning and the risk assessment of LH_2 tanks. The following section generalizes and systematizes such considerations analyzing the outcome of the MLI system performance assessment presented in Section 3.3.

5.2. Assessment of MLI performance effectiveness under fire exposure

Fig. 5 reports the values of *DIF* and *DIP* (defined in Section 3.3) as a function of the exposure time (data showed with a step of 300 s) for the reference fire scenarios considered in this study. Fig. 5a and c refer to aluminum-based MLI, while Fig. 5b and d refer to polyester-based MLI.

As the figure clearly shows, in the case of severe fires (ψ_f from 0.8 to 1), the *DIF* values evidence that the capacity of both MLIs to insulate the tank degrades within the first 10–15 min of exposure (see Fig. 5a and b). For longer times, $k_{eff,F}$ increases by several orders of magnitude with respect to normal operating conditions (4 for aluminum-based MLIs, 5

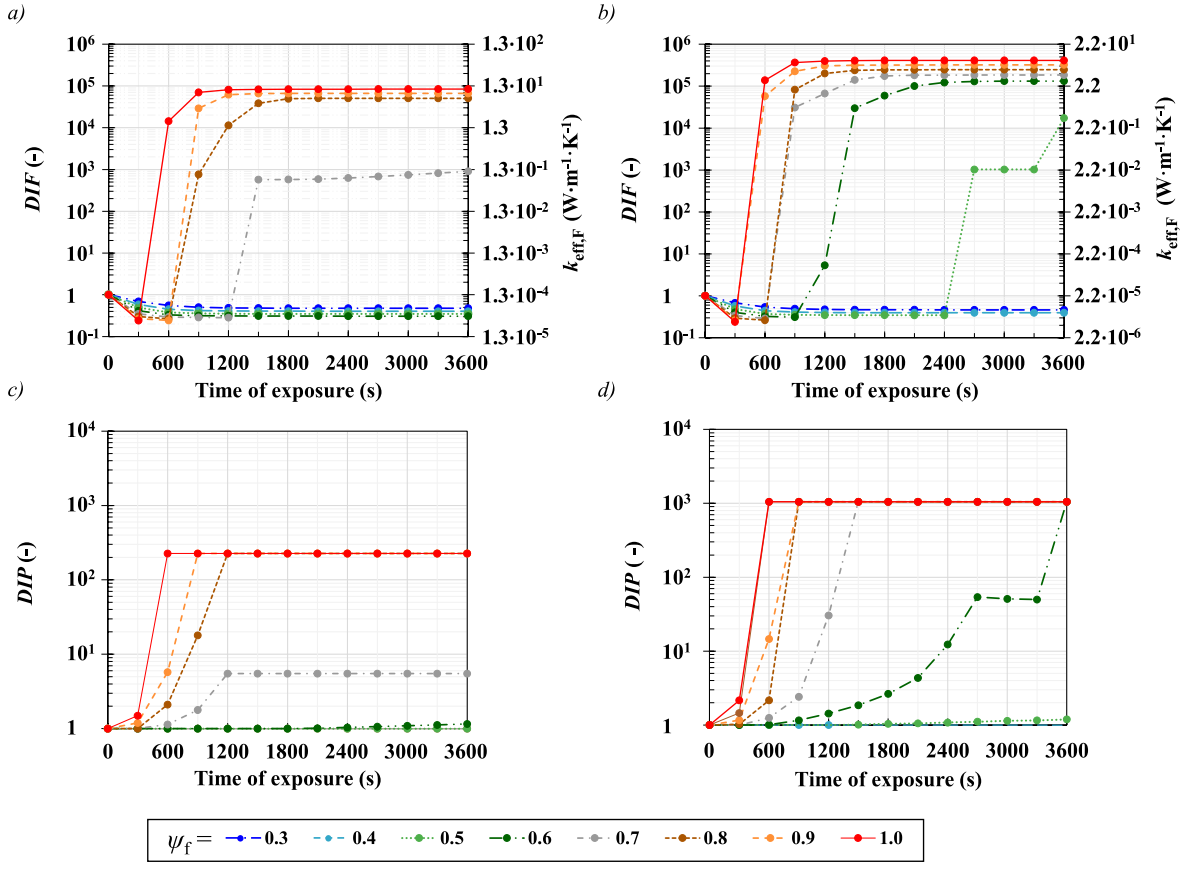

Fig. 5. Values of the DIF and DIP KPIs calculated for aluminum-based MLI (panels a and c) and polyester-based MLI (panels b and d) as a function of time of exposure for different ψ_f factors characterizing the fire scenarios as reported in Fig. 3 (the severity of fire intensity increases with ψ_f). The corresponding value of the effective thermal conductivity of the insulation in fire conditions ($k_{eff,F}$) when considering DIF is shown on the right y-axis.

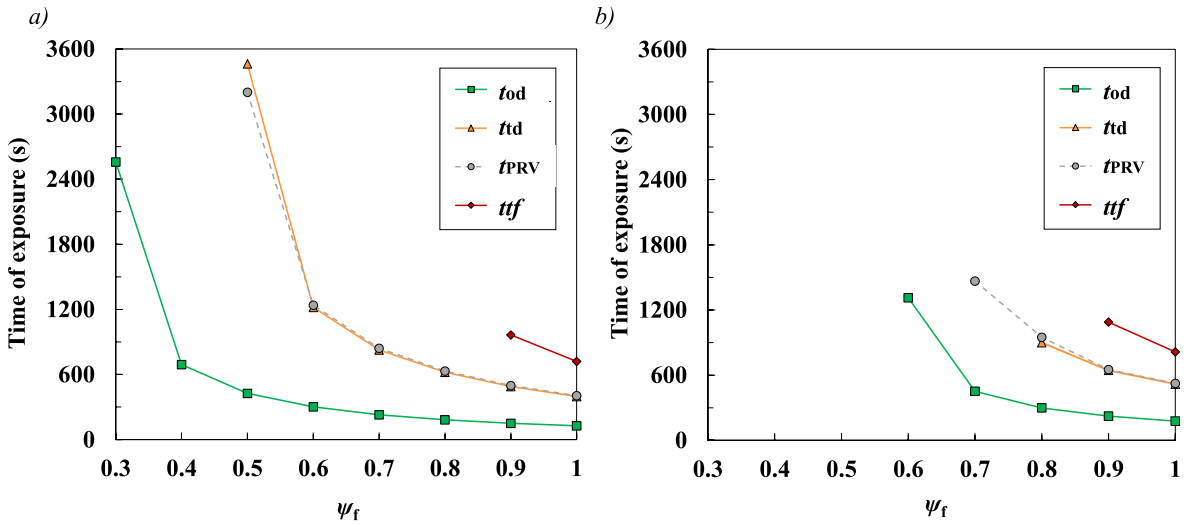

Fig. 6. Values of Reference Times (RTs, see section 2.4) reported versus fire exposure time and ψ_f factors characterizing the fire scenarios as reported in Fig. 3 (the severity of fire intensity increases with ψ_f). Panel a refers to polyester-based MLI while Panel b to aluminum-based one. The absence of RT marker(s) indicates that the relevant event(s) does not occur for the specific value of ψ_f during the 3600 s (60 min) of fire exposure.

for polyester-based MLIs). The maximum thermal conductivity values reached under fire exposure are 12 W/(m·K) and 16 W/(m·K) for aluminum-based and polyester-based materials, respectively. The *DIP* indicates that, in the fire aftermath (i.e. when the tank is exposed again to atmospheric conditions), the value of $k_{eff,F}$ for aluminum-based MLIs is up to 200 times higher compared to that before thermal exposure. The *DIP* value reaches 1000 for polyester-based MLIs. In terms of insulation performance degradation, this is comparable with the effect of loss of vacuum within the double wall, which is recognized to increase the effective thermal conductivity by 2–3 orders of magnitude [27].

At lower fire intensities, the two MLI systems show a more pronounced difference in fire resistance. The Aluminum-based MLI is only partially affected when $\psi_f = 0.7$, while almost no degradation at lower values. In practice, for $\psi_f \leq 0.6$, the calculated *DIF* and *DIP* values (DIF values lower than 1 are due to the simplifications introduced by the definition of $k_{eff,F}$) indicate that the insulation performance during and after fire exposure is close to that of a system before thermal exposure. On the other hand, the insulation capacity of Polyester-based MLI drops severely also for $\psi_f = 0.6$ (0.5 if the fire lasts more than 2700 s), and only when $\psi_f \leq 0.4$ does the degree of fire-induced degradation become negligible.

These results are reflected in the outcome of the analysis of the reference times (RTs) identified in Section 3.3. The values calculated are reported in Fig. 6 as a function of the exposure time and of the fire scenario, defined by the ψ_f parameter.

In the case of aluminum-based MLI, the fire scenarios characterized by $\psi_f \leq 0.5$ induce no damage to the insulation system, while t_{od} drops quickly in more severe fire scenarios. On the contrary, polyester-based MLI appears more vulnerable, with much smaller t_{od}. For example, for $\psi_f = 0.4$, the first degradation appears already after 660 s (11 min). For both MLI systems, the time of total degradation (t_{td}) follows t_{od} by a time lag decreasing as ψ_f increases. In most of the cases, the first opening of the PRV occurs immediately after t_{td}. As in the case of the t_{od}, the t_{td} and the t_{PRV} obtained for aluminum-based MLI are lower than those calculated for polyester-based one.

On the contrary, the values of *ttf* are quite similar. Tank failure is observed only for the two most severe fire conditions (i.e., for ψ_f equal to 0.9 and 1). In both cases and for both MLI types, this occurs after the insulation system is destroyed (i.e., $ttf > t_{td}$). On the contrary, the results obtained for $\psi_f \leq 0.8$ show that the total degradation of the MLI does not always imply that the tank failure will follow. This suggests that, for a given exposure time, a threshold value for ψ_f (and thus for the flame temperature) exists below which failure does not occur. For an exposure time of 3600 s (60 min), this is comprised between 0.9 and 0.8. These findings are further discussed in Section 5.3.

5.3. The influence of external shell temperature on the thermal insulation performance

The results illustrated in the previous sections indicate that both polyester- and aluminum-based MLI systems undergo severe degradation when exposed to realistic fire scenarios and provide thermal protection to the tank for a limited period of time. The *ttf* as well as the other RTs depend on the severity of the fire scenario (i.e. on the value of ψ_f) and, ultimately, on the flame temperature. The flame temperature is one of the most relevant factors that characterize the fire intensity and is considered in several standards as a target parameter to define the fire testing conditions of superinsulated tanks [69–72]. However, the fire temperature alone is not sufficient to quantify the heat flux to an object (e.g. an LH_2 tank) exposed to fire. As reported in Eq.s (37)–(39), the emissivity of the fire and of the external wall, as well as the flame heat transfer coefficient also play a relevant role [56]. Different values of heat flux can thus result from fires featuring the same flame temperature.

Therefore, in order to provide a systematic definition of threshold temperature conditions that are independent of the several parameters characterizing a specific fire scenario, the external shell temperature (T_{Se}) is considered as the reference for the discussion that follows. This approach presents two main advantages.

- It allows the calculation of the heat flux to the tank on the basis of a single value of temperature (T_{Se}) as a boundary condition, eliminating the uncertainties related to the fire characteristics;
- The value of T_{Se} is easily and reliably measurable during fire tests compared to the flame temperature.

Fig. 7 illustrates the impact of T_{Se} on the four RTs defined in Section 3.3. The charts were obtained as the outcome of 900 simulations run by varying the temperature of the external shell in the interval 573–1373 K with steps of 1 K. T_{Se} was kept constant in each simulation.

The results show that for external shell temperatures above 1157 K, the failure of the tank occurs within a few minutes (less than 19 min, 1140 s). Such temperatures are similar to those measured in real-scale

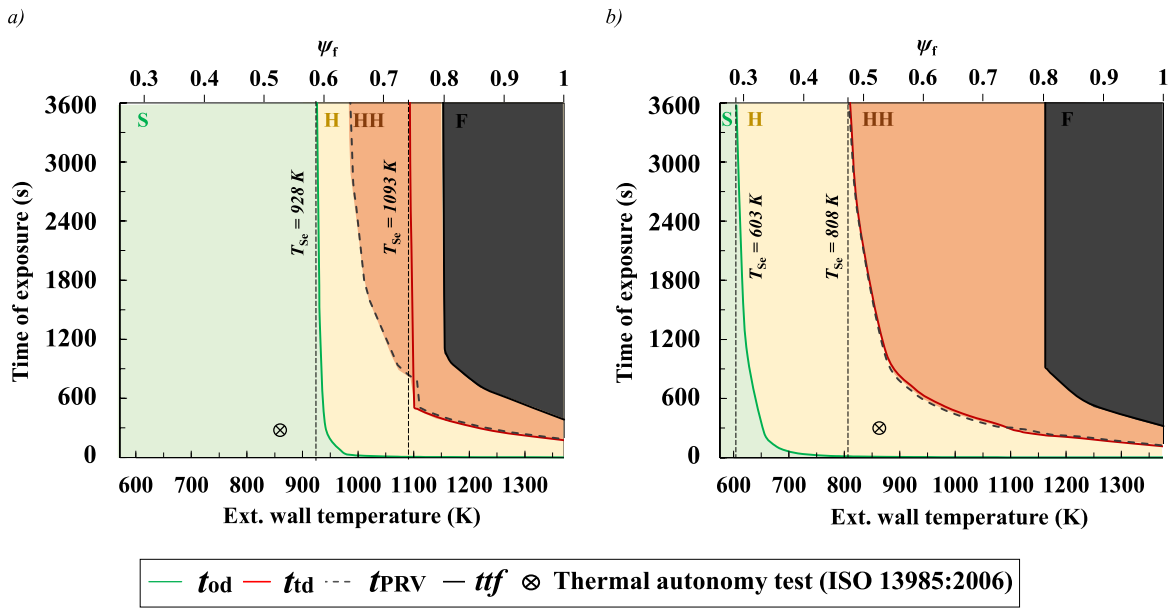

Fig. 7. Values calculated for the Reference times versus the fire exposure time considering a constant temperature of the external wall of the tank (the corresponding flame temperature factors, ψ_f, are reported on the upper x-axis). (a) aluminum-based MLI; (b) polyester-based MLI.

fire tests involving cryogenic tanks [15,73], thus representing credible fire scenarios. In such conditions, the MLI systems completely degrade within a maximum of 360 s (6 min), leaving the tank unprotected. On the contrary, the degradation is significantly delayed ($t_{td} > 3600$ s) when T_{Se} is lower than 808 K for polyester-based MLI and 1093 K for aluminum-based one, while it can be considered to be avoided ($t_{od} >$ 3600 s) for wall temperatures not exceeding 608 K for polyester-based MLIs and 928 K aluminum-based MLIs.

From a safety standpoint, the t_{od}, t_{td}, t_{PRV}, and *ttf* curves in Fig. 7 identify 4 regions that can be used to assess the hazard of given fire scenarios. On the basis of the conservative assumption that T_{Se} reaches immediately the fire temperature, scenarios for which the fire is suppressed before t_{od} can be deemed safe (S, green shaded region). On the other hand, fires engulfing the tank longer than t_{od} can lead to different outcomes, which depend on the duration of the fire. In the worst case, the MLI is completely degraded, followed by rapid pressurization and consequent tank failure. Exposure times longer than *ttf* identify the failure zone (F, black-shaded region), representing the most severe evolution of the fire accident, with dramatic consequences for people, vehicles, and structures nearby.

For exposure times lower than *ttf*, a highly hazardous (HH) region, identified by the orange-shaded area in Fig. 7, is defined where t_{td} or t_{PRV} (the lowest one for the case considered) is reached. In this scenario, the PRV opening has already happened or is about to take place. If the released fluid is flammable, as in the case of hydrogen, this can generate a jet fire.

Finally, a region where a lower hazard is present (H) is yellow-shaded in Fig. 7, delimited by the t_{od} and the lowest between t_{PRV} and t_{td} curves. In this region the MLI system is partially damaged. Although the failure of the system as well as dangerous releases can be excluded in this situation, unsafe scenarios related to self-pressurization more rapid than in normal operating conditions cannot be ruled out in the fire aftermath.

The model application oriented to the identification of the temperatures bounding the safety zones and their extension represents an innovative methodology for the assessment and comparison of thermal performances of insulation material for LH_2 tanks under fire scenarios. This can potentially be extended to LNG (and other cryogenic fluids) tanks.

5.4. Discussion

The above results show that the KPIs proposed, and in particular the quantification of the RTs, provide valuable insights into the MLI performances and tank resistance to fire, offering key information for emergency planning: the later these events occur, the higher the time available for responders to mitigate the fire and prevent severe escalation. Overall, the KPIs and RTs analysis provide useful and valuable metrics for the assessment of thermal insulation performance under fire conditions.

The results of the sensitivity analysis, reported in Section D of the Supplementary Material, confirm the robustness of the model. The model output variation is always lower than 5 % when considering a ±10 % variation of the parameters listed in Table 6 with respect to the reference values used in the model.

The results also highlight the strong connection between the safety of LH_2 tanks and the integrity of the MLI materials during fire exposure. An intact or partially damaged MLI effectively prevents tank failure and delays hazardous hydrogen releases within a period that allows the effective application of fire mitigation measures. However, when the MLI completely degrades, the scenario changes dramatically, with a high risk of hydrogen release and tank failure. These results suggest that an inherently safe MLI-equipped LH_2 tank shall feature an insulation system able to withstand all the fire scenarios that are credible for a given application.

According to the ISO 13985:2006 [34], an MLI-insulated LH_2 storage tank for mobile applications is accepted for use on the basis of a thermal autonomy test under specific fire conditions. This is performed by exposing the tank (as designed for final application) to a fire with an average temperature of the space 10 mm below the tank of at least 863 K until the blow-off of the pressure relief valve is completed. The insulation system is deemed acceptable if the time required for the inner tank pressure to rise from a starting pressure equal to the saturation pressure of hydrogen in the tank (atmospheric pressure in the present study) to the value of the first PRV opening is equal to or higher than 300 s (5 min). Similar requirements are defined in regulations for the approval of LH_2 and LNG tanks [37,74]. However, when looking at Fig. 7, the fire scenario prescribed by ISO 13985:2006 [34] (which is represented by the crossed dot in Fig. 7) would produce no effect on the LH_2 tank taken as reference in the present study if this was equipped with the

aluminum-based MLI system described in Table 5, while it would partially damage the tank equipped with polyester-based MLI. In both cases, the PRV would not be activated. Thus, both insulation systems would pass the ISO 13985:2006 thermal autonomy test. However, Fig. 7 shows that exposing the tank (with either MLI system) to more severe, yet credible fire scenarios, could result in very unsafe or even failure conditions.

Therefore, these findings provide key insights for the fire safety improvement of LH_2 mobile tanks. A first issue concerns the need for the revision and improvement of the current standard fire testing conditions based on a comprehensive characterization of the typical fire scenarios that can involve LH_2 tanks (depending on the application sector).

A second issue concerns the resistance of MLI materials to fire scenarios. The results obtained show that the most widely adopted MLI materials, which are based on polyester, may not withstand all the potential fire accident scenarios involving LH_2 storage and transportation tanks. However, keeping the external shell temperature under control during fire exposure can effectively ensure the safety of cryogenic liquid tanks equipped with MLI. In this perspective, the application of fire-proofing to the tank outer shell may represent an effective solution to preserve the MLI system performance both during and after the fire. Future research efforts should focus on exploring innovative MLIs, including hybrid systems made of fire-resistant materials with higher degradation temperatures to improve performance in severe conditions. These improvements may contribute to prolonging the time available to emergency response teams to suppress the fire and evacuate the personnel, and avoid pressure relief devices activation in the fire aftermath. In this framework, the time to first PRV opening (t_{PRV}) calculated by the proposed model may represent a key parameter for rescue teams as it suggests the maximum evacuation time before the PRV release and, even worse, the catastrophic failure of the tank occurs.

Focusing on the modeling approach developed, it is important to highlight a few issues. The first concerns the validation of the model. This relies on experimental data on MLI degradation [24,25] and cryogenic liquid tank pressurization at a lab scale [75,76]. Unfortunately, measurements from liquid hydrogen fire tests available in the literature lack the level of detail required for a more comprehensive validation of the approach (see Section 3.2). A further consideration regards the effect of the pressure in the gap between the inner and outer walls. Experiments have shown that MLI degradation during fire exposure may come together with the generation of gaseous decomposition products and consequent vacuum loss [24]. This may cause a transition in the heat transfer regime from being dominated by radiation to being dominated by gas convection. Although the proposed model may account for this transition (based on the value of the pressure), it is not able to predict how the pressure evolves within the gap (more details on this aspect can be found in Ref. [24]). This is due to the lack of correlations linking the amount of gaseous compounds generated during the MLI degradation process. For this reason, the loss of vacuum was not explored in the present study and it was assumed that the pressure remains constant. For what concerns the tank pressurization, the model neglects thermal stratification effects. This assumption is reasonable for small-size tanks, such as those used in hydrogen-fuelled vehicles (e.g. heavy-duty trucks) and analysed in the present study, for which the effect of stratification is negligible [39,40]. For larger tanks (such as those for static storage or bulk transportation), the stratification accelerates the pressurization, but it tends to vanish when the PRV activates [41,42]. Based on this, it is possible to expect that the proposed model may underestimate the pressurization rate before PRV activation when applied to large tanks. Therefore, its reliability is mainly limited to small-scale liquid hydrogen (LH_2) storage tanks. It is also worth mentioning that the model assumes a uniform full engulfment fire condition. Thus, the use of the model to analyse localized fire scenarios would produce conservative results.

The tank geometry and insulation properties considered for the case study (see Sections 4.1 and 4.2) are representative of the most common solutions adopted in LH2-fuelled tanks. The sensitivity of the model results to the variation of the input parameters was assessed and the results are presented in Section S.D of the Supplementary Material. The outcomes of the analysis demonstrate the robustness of the modelling approach.

Although the quantitative results reported in Section 5 refer to the specific case study analysed, the methodology proposed for the performance assessment of the MLI systems has a general validity. Actually, the model may consider both different MLI geometries (for instance, different numbers of layers and layer density, also including variable density MLIs [77]) and materials (upon characterization of the proper degradation kinetics [24]). Moreover, MLI systems combined with vapor-cooled shields (VCS) may also be addressed by incorporating one or more thermal nodes in the model, depending on the system type, to account for the energy sink represented by the VCS [78]. Finally, the approach can be applied to tanks with different storage conditions (for instance, different liquid levels and storage pressure). All these aspects demonstrate the robustness and flexibility of the novel methodology proposed in this study.

6. Conclusions

The present study proposes an innovative approach to the comparative assessment of the thermal performance of typical MLI systems for LH_2 cryogenic tanks under full engulfment fires. This was achieved by coupling heat transfer and thermal degradation models for the MLI system with a lumped model developed for this purpose.

The outcome of the case study, based on a vehicle scale LH_2 tank in a full engulfing pool fire scenario evidenced that aluminum-based MLIs feature superior fire resistance to polyester-based ones. However, both aluminum-based and polyester-based MLIs degrade severely when typical hydrocarbon pool fire conditions are considered, leaving the tank unprotected in 300–900 s (5–15 min) of exposure and inducing tank failure despite the activation of the PRV. Compliance with the acceptance criteria based on the thermal autonomy test proposed by ISO 13985:2006 [34] does not ensure the survival of the tank in realistic fire scenarios. These results emphasize the key role that MLI systems play in the response of cryogenic tanks to fire exposure, the understanding of which is paramount to improving the safety of LH_2-powered vehicle safety and assisting emergency planning.

The original approach developed in the present study represents an innovative method for the assessment of fire scenarios affecting LH_2 tanks equipped with MLI systems. The identification of failure and hazard regions provided by the approach can be used in early design stages to select the safest solutions and identify appropriate protection measures. The reference times defined also provide valuable information to support emergency response planning in case of fire accidents.

Overall, the approach developed provides specific tools able to support the design and risk assessment of cryogenic tanks for liquefied hydrogen storage.

CRediT authorship contribution statement

Davide Camplese: Writing – original draft, Methodology, Investigation, Formal analysis, Data curation, Conceptualization. **Giordano Emrys Scarponi:** Writing – original draft, Validation, Methodology, Investigation, Formal analysis, Conceptualization. **Robert Eberwein:** Writing – review & editing, Validation, Investigation, Data curation, Conceptualization. **Aliasghar Hajhariri:** Investigation, Formal analysis, Data curation, Conceptualization. **Frank Otremba:** Supervision, Investigation, Conceptualization. **Valerio Cozzani:** Writing – review & editing, Validation, Investigation, Formal analysis, Conceptualization.

Declaration of competing interest

The authors declare that they have no known competing financial interests or personal relationships that could have appeared to influence

the work reported in this paper.

Acknowledgments

Funding received from the Italian Ministry of University and Research under the National Recovery and Resilience Plan, Misson 4, Component 2, Investment 1.3, NextGenerationEU, Project “Network 4 Energy Sustainable Transition”, PE00000021, CUPJ33C22002890007 is gratefully acknowledged.

Appendix A. Supplementary data

Supplementary data to this article can be found online at https://doi.org/10.1016/j.ijhydene.2025.04.534.

References

[1] Cipriani G, Di Dio V, Genduso F, La Cascia D, Liga R, Miceli R, et al. Perspective on hydrogen energy carrier and its automotive applications. Int J Hydrogen Energy 2014;39:8482–94. https://doi.org/10.1016/j.ijhydene.2014.03.174.
[2] Kovač A, Paranos M, Marciuš D. Hydrogen in energy transition: a review. Int J Hydrogen Energy 2021;46:10016–35. https://doi.org/10.1016/j.ijhydene.2020.11.256.
[3] Kunze K, Kircher O. Cryo-compressed hydrogen storage cryogenic cluster day. Sept 2012;28:2012. Oxford.
[4] Peschka W. Liquid hydrogen: fuel of the future. Springer Science & Business Media; 2012.
[5] Yin L, Yang H, Ju Y. Review on the key technologies and future development of insulation structure for liquid hydrogen storage tanks. Int J Hydrogen Energy 2024;57:1302–15. https://doi.org/10.1016/j.ijhydene.2024.01.093.
[6] Edward L, Filip L. Influence of vacuum level on insulation thermal performance for LNG cryogenic road tankers. MATEC Web Conf. 2018;240:1019. EDP Sciences.
[7] Ahluwalia RK, Roh HS, Peng JK, Papadias D, Baird AR, Hecht ES, et al. Liquid hydrogen storage system for heavy duty trucks: configuration, performance, cost, and safety. Int J Hydrogen Energy 2023;48:13308–23. https://doi.org/10.1016/j.ijhydene.2022.12.152.
[8] Schiaroli A, Scarponi GE, Antonioni G, Cozzani V. Hazard footprint of alternative fuel storage concepts for hydrogen-powered urban buses. Int J Hydrogen Energy 2024;50:1430–42. https://doi.org/10.1016/j.ijhydene.2023.11.104.
[9] Sánchez AL, Williams FA. Recent advances in understanding of flammability characteristics of hydrogen. Prog Energy Combust Sci 2014;41:1–55. https://doi.org/10.1016/j.pecs.2013.10.002.
[10] Li Z, Pan X, Meng X, Ma J. Study on the harm effects of releases from liquid hydrogen tank by consequence modeling. Int J Hydrogen Energy 2012;37:17624–9. https://doi.org/10.1016/j.ijhydene.2012.05.141.
[11] Hu Q, Zhang X, Hao H. A review of hydrogen-air cloud explosions: the fundamentals, overpressure prediction methods, and influencing factors. Int J Hydrogen Energy 2023;48:13705–30. https://doi.org/10.1016/j.ijhydene.2022.11.302.
[12] Zhang A, Shen J, Gao W. Investigation on the morphology and temperature distribution of hydrogen jet flames impinging on barrier walls. Int J Hydrogen Energy 2024;79:741–55. https://doi.org/10.1016/j.ijhydene.2024.07.077.
[13] Wu Z, Cheng Q, Gu X, Wang Z, Lu L, Pan X, et al. Experimental investigation on the development characteristics of high-pressure hydrogen jet flame under different ignition conditions. Int J Hydrogen Energy 2024;79:791–801. https://doi.org/10.1016/j.ijhydene.2024.07.053.
[14] Reniers G, Cozzani V. Domino effects in the process industries: modelling, prevention and managing. Newnes; 2013.
[15] Pehr K. Experimental examinations on the worst case behavior of LH2/LNG tanks for passenger cars. Proc. 11th World Hydrog. Energy Conf. Stuttgart, Ger. 1996:2169–86.
[16] van Wingerden K, Kluge M, Habib AK, Ustolin F, Paltrinieri N. Medium-scale tests to investigate the possibility and effects of BLEVEs of storage vessels containing liquified hydrogen. Chem Eng Trans 2022;90:547–52. https://doi.org/10.3303/CET2290092.
[17] Abbasi T, Abbasi SA. The boiling liquid expanding vapour explosion (BLEVE): mechanism, consequence assessment, management. J Hazard Mater 2007;141:489–519. https://doi.org/10.1016/j.jhazmat.2006.09.056.
[18] Zalosh R, Weyandt N. Hydrogen fuel tank fire exposure burst test. SAE Trans 2005:2338–43.
[19] Eberwein R, Hajhariri A, Camplese D, Emrys Scarponi G, Cozzani V, Otremba F. Insulation materials used in tanks for the storage of cryogenic fluids in fire scenarios. American Society of Mechanical Engineers; 2023. https://doi.org/10.1115/PVP2023-105201. Vol. 6 Oper. Appl. Components.
[20] Eberwein R, Hajhariri A, Camplese D, Scarponi GE, Cozzani V, Otremba F. Experimental investigation on the behavior of thermal super insulation materials for cryogenic storage tanks in fire incidents. Process Saf Environ Prot 2024;187:240–8. https://doi.org/10.1016/j.psep.2024.04.131.
[21] Eberwein R, Hajhariri A, Camplese D, Scarponi GE, Cozzani V, Otremba F. Experimental research of A tank for A cryogenic fluid with A wall rupture in A fire scenario. 15th ISHPMIE, Naples 2024. https://doi.org/10.5281/zenodo.12621001.
[22] Scarponi GE, Landucci G, Ovidi F, Cozzani V. Lumped model for the assessment of the thermal and mechanical response of LNG tanks exposed to fire. Chem Eng Trans 2016;53:307–12. https://doi.org/10.3303/CET1653052.
[23] Ustolin F, Scarponi GE, Iannaccone T, Cozzani V, Paltrinieri N. Cryogenic hydrogen storage tanks exposed to fires: a CFD study. Chem Eng Trans 2022;90:535–40. https://doi.org/10.3303/CET2290090.
[24] Camplese D, Scarponi GE, Chianese C, Hajhariri A, Eberwein R, Otremba F, et al. Modeling the performance of multilayer insulation in cryogenic tanks undergoing external fire scenarios. Process Saf Environ Prot 2024;186:1169–82. https://doi.org/10.1016/j.psep.2024.04.061.
[25] Hajhariri A, Eberwein R, Camplese D, Scarponi GE, Cozzani V, Otremba F, et al. Non-combustible MLI based insulation behavior under fire condition - experimental and numerical investigation. Process Saf Environ Prot 2024. https://doi.org/10.1016/j.psep.2024.11.037.
[26] Camplese D, Chianese C, Scarponi GE, Eberwein R, Otremba F, Cozzani V. Analysis of high temperature degradation of multi-layer insulation (MLI) systems for liquid hydrogen storage tanks. Chem Eng Trans 2023;99:415–20. https://doi.org/10.3303/CET2399070. SE-Research Articles.
[27] American Society for Testing and Materials. Standard guide for evacuated reflective insulation in cryogenic service. ASTM C740/740M-13); 2019.
[28] Fesmire JE, Johnson WL. Cylindrical cryogenic calorimeter testing of six types of multilayer insulation systems. Cryogenics 2018;89:58–75. https://doi.org/10.1016/j.cryogenics.2017.11.004.
[29] Li K, Chen J, Tian X, He Y. Study on the performance of variable density multilayer insulation in liquid hydrogen temperature region. Energies 2022;15:9267. https://doi.org/10.3390/en15249267.
[30] Martin JJ, Hastings L. Large-scale liquid hydrogen testing of variable density multilayer insulation with a foam substrate. 2001.
[31] Fesmire JE. Standardization in cryogenic insulation systems testing and performance data. Phys Procedia 2015;67:1089–97. https://doi.org/10.1016/j.phpro.2015.06.205.
[32] Wang P, Ji L, Yuan J, An Z, Yan K, Zhang J. Modeling and optimization of composite thermal insulation system with HGMs and VDMLI for liquid hydrogen on orbit storage. Int J Hydrogen Energy 2020;45:7088–97. https://doi.org/10.1016/j.ijhydene.2019.12.110.
[33] Hastings LJ, Flachbart RH, Martin JJ, Hedayat A, Fazah M, Lak T, et al. Spray bar zero-gravity vent system for on-orbit liquid hydrogen storage. 2003.
[34] International Organization for Standardization (ISO). ISO 13985:2006 – Liquid hydrogen — Land vehicle fuel tanks. Geneva, Switzerland: ISO; 2006.
[35] United Nations. Agreement concerning the international carriage of dangerous goods by road (ADR). ECE/TRANS/300 2020;II.
[36] ASTM-C1774. Standard guide for thermal performance testing of cryogenic insulation systems. ASTM Int 2013;13:1–23. https://doi.org/10.1520/C1774-13.2.
[37] United Nations. GTR 13 Global technical regulation on hydrogen and fuel cell vehicles. 2013.
[38] NIST. NIST chemistry WebBook 69. National Institute for Standards and Technology; 2019. https://webbook.nist.gov/chemistry/. [Accessed 22 July 2024].
[39] Dancer D, Sallet DW. Pressure and temperature response of liquefied gases in containers and pressure vessels which are subjected to accidental heat input. J Hazard Mater 1990;25:3–18. https://doi.org/10.1016/0304-3894(90)85066-C.
[40] Scarponi GE, Landucci G, Birk AM, Cozzani V. LPG vessels exposed to fire: scale effects on pressure build-up. J Loss Prev Process Ind 2018;56:342–58. https://doi.org/10.1016/j.jlp.2018.09.015.
[41] Birk AM, Cunningham MH. Liquid temperature stratification and its effect on BLEVEs and their hazards. J Hazard Mater 1996;48:219–37. https://doi.org/10.1016/0304-3894(95)00157-3.
[42] Aydemir NU, Magapu VK, Sousa ACM, Venart JES. Thermal response analysis of LPG tanks exposed to fire. J Hazard Mater 1988;20:239–62. https://doi.org/10.1016/0304-3894(88)87015-8.
[43] Van Den Bosh CJH, Weterings R. TNO Yellow Book, Methods for the calculation of physical effects. 2005.
[44] Wang L, Li Y, Zhang F, Xie F, Ma Y. Correlations for calculating heat transfer of hydrogen pool boiling. Int J Hydrogen Energy 2016;41:17118–31. https://doi.org/10.1016/j.ijhydene.2016.06.254.
[45] Churchill SW, Usagi R. A general expression for the correlation of rates of transfer and other phenomena. AIChE J 1972;18:1121–8.
[46] International Organization for Standardization. Cryogenic vessels — pressure-relief accessories for cryogenic service Part 3 : sizing and capacity determination (ISO 21013-3:2016. 2016.
[47] Bell IH, Wronski J, Quoilin S, Lemort V. Pure and Pseudo-pure fluid thermophysical property evaluation and the open-source thermophysical property library CoolProp. Ind \& Eng Chem Res 2014;53:2498–508. https://doi.org/10.1021/ie4033999.
[48] Leachman JW, Jacobsen RT, Penoncello SG, Lemmon EW. Fundamental equations of state for parahydrogen, normal hydrogen, and orthohydrogen. J Phys Chem Ref Data 2009;38:721–48. https://doi.org/10.1063/1.3160306.
[49] Hadjisophocleous GV, Sousa ACM, Venart JES. A study of the effect of the tank diameter on the thermal stratification in LPG tanks subjected to fire engulfment. J Hazard Mater 1990;25:19–31. https://doi.org/10.1016/0304-3894(90)85067-D.
[50] Venart JES. Boiling liquid expanding vapour explosions (BLEVE); possible failure mechanisms and their consequences. Inst Chem Eng Symp Ser 2000;147:121–38. Institution of Chemical Engineers; 1999.
[51] International Organization for Standardization. Cryogenic vessels — cryogenic insulation performance. 2019 (ISO 21014:2019).

[52] Al Ghafri SZS, Swanger A, Jusko V, Siahvashi A, Perez F, Johns ML, et al. Modelling of liquid hydrogen boil-off. Energies 2022;15:1149. https://doi.org/10.3390/en15031149.
[53] Jeon G-M, Jeong S-M, Park J-C. Experimental and numerical investigation of the influences of sloshing motion on the change in boil-off gas/boil-off rate in a cryogenic liquid tank. Ocean Eng 2024;298:117173. https://doi.org/10.1016/j.oceaneng.2024.117173.
[54] Vullo V. Circular cylinders and pressure vessels stress analysis and design. Springer; 2014.
[55] European Committee for Standardization. Eurocode 3 - design of steel structures. Part 1-2: structural fire design. 2024. EN 1993-1-2:2024).
[56] International Organization for Standardization. Determination of the resistance to hydrocarbon pool fires of fire protection materials and systems for pressure vessels (ISO Standard No. 21843:2023). 2023.
[57] Patankar SV. Numerical heat transfer and fluid flow/Suhas V. Patankar. Hemisphere Pub. Corp. ; McGraw-Hill; 1980. Washington : New York.
[58] Key to Metals AG. Total Materia - the world's most comprehensive Materials database. https://portal.totalmateria.com. [Accessed 15 July 2023].
[59] European Committee for Standardization (CEN). EN 1993-1-4:2006 – Eurocode 3: Design of steel structures – Part 1-4: General rules – Supplementary rules for stainless steels. Brussels, Belgium: CEN; 2006.
[60] International Organization for Standardization. Cryogenic vessels — static vacuum insulated vessels. 2022. ISO 21009-1:2022.
[61] Iannaccone T, Landucci G, Scarponi GE, Bonvicini S, Cozzani V. Inherent safety assessment of alternative technologies for LNG ships bunkering. Ocean Eng 2019;185:100–14. https://doi.org/10.1016/j.oceaneng.2019.05.028.
[62] ASTM. Standard practice for evacuated reflective insulation in cryogenic service 1. Astm 2015;82:1–9. https://doi.org/10.1520/C0740-97.
[63] European Committee for Standardization. Designation systems for steels Part 2 : Numerical system (en 10027-2:2015). 2015.
[64] Davis JR, editor. ASM specialty handbook: stainless steels. ASM International; 1994.
[65] Bartl J, Baranek M. Emissivity of aluminium and its importance for radiometric measurement. Meas Sci Rev 2004;4:31–6.
[66] Rüdiger H. Design characteristics and performance of a liquid hydrogen tank system for motor cars. Cryogenics (Guildf) 1992;32:327–9. https://doi.org/10.1016/0011-2275(92)90373-I.
[67] Scarponi GE, Landucci G, Birk AM, Cozzani V. Three dimensional CFD simulation of LPG tanks exposed to partially engulfing pool fires. Process Saf Environ Prot 2021;150:385–99. https://doi.org/10.1016/j.psep.2021.04.026.
[68] Bradley I, Scarponi GE, Otremba F, Birk AM. An overview of test standards and regulations relevant to the fire testing of pressure vessels. Process Saf Environ Prot 2021;145:150–6. https://doi.org/10.1016/j.psep.2020.07.047.
[69] German Institute for Standardisation (Deutsches Institut für Normung). Engineering structures in connection with roads - inspection and test (DIN 1076: 1999-11). 1999.
[70] European Committee for Standardization. Fire resistance tests—Part 2: alternative and additional procedures. 1999. EN 1363-2).
[71] BASt (Bundesanstalt für Straßenwesen). Zusätzliche Technische Vertragsbedingungen und Richtlinien für Ingenieurbauten (ZTV-ING) Teil 5 "Tunnelbau" und Teil 3 "Massivbau". 2015. Abschnitt 1 "Beton.
[72] International Organization for Standardization. Fire resistance tests (ISO Standard N. 834). 1999.
[73] Kamperveen JP, Spruijt MPN, Reinders JEA. Heat load resistance of cryogenic storage tanks–Results of LNG Safety Program. 2016. Utrecht, The Netherlands.
[74] United Nations Economic Commission for Europe (UNECE). UN regulation No. 110 Rev.6. Off J Eur Union 2022:207.
[75] Xie GF, Li XD, Wang RS. Experimental study on the storage performance of high-vacuum-multilayer- insulation tank after sudden, catastrophic loss of insulating vacuum. Heat Mass Transf Und Stoffuebertragung 2012;48:757–66. https://doi.org/10.1007/s00231-011-0928-z.
[76] Xie GF, Li XD, Wang RS. Study on the heat transfer of high-vacuum-multilayer-insulation tank after sudden, catastrophic loss of insulating vacuum. Cryogenics (Guildf) 2010;50:682–7. https://doi.org/10.1016/j.cryogenics.2010.06.020.
[77] Wang B, Huang YH, Li P, Sun PJ, Chen ZC, Wu JY. Optimization of variable density multilayer insulation for cryogenic application and experimental validation. Cryogenics (Guildf) 2016;80:154–63. https://doi.org/10.1016/j.cryogenics.2016.10.006.
[78] Jiang W, Zuo Z, Sun P, Li P, Huang Y. Thermal analysis of coupled vapor-cooling-shield insulation for liquid hydrogen-oxygen pair storage. Int J Hydrogen Energy 2022;47:8000–14. https://doi.org/10.1016/j.ijhydene.2021.12.103.